Arctic sediment routing during the Triassic: sinking the Arctic Atlantis

Albina Gilmullina[1]*, Tore Grane Klausen[2], Anthony George Doré[3], Hallgeir Sirevaag[1], Anna Suslova[4] and Christian Haug Eide[1]

[1] Department of Earth Science, University of Bergen, Allégaten 41, 5007 Bergen, Norway
[2] M Vest Energy AS, Edvard Griegs vei 3, 5059 Bergen, Norway
[3] Energy & Geoscience Institute (EGI), University of Utah, 423 Wakara Way, Suite 300, Salt Lake City, UT 84108, USA
[4] Petroleum Department, Lomonosov Moscow State University, 1 Leninskiye Gory, 119991 Moscow, Russia
   AG, 0000-0001-6187-9029; TGK, 0000-0003-2524-512X; HS, 0000-0001-8195-3505; CHE, 0000-0003-4949-9917
* Correspondence: albina.gilmullina@uib.no

Abstract: Opening of the Arctic Ocean has been the subject of much debate, and the placement of terranes in the Early Mesozoic remains a crucial part of this important discussion. Several continental terranes complicate the palaeogeographical reconstruction. One such terrane is Crockerland, which has been inferred to explain sediment distribution in the Arctic throughout the Mesozoic. However, Triassic successions throughout the Arctic basins bear many similarities, and a common sedimentary source could offer a simpler explanation with fewer complications for the past configuration of the Arctic. The study's goal is to test the hypothesis of long-distance sediment transport from a common source in present-day Russia to all Arctic basins in the Triassic, and to demonstrate how estimates of sediment routing distances can improve pre-break-up plate-tectonic reconstructions. Results confirm that (1) the Arctic basins were closely connected prior to break-up in the Mesozoic, (2) based on regional facies distribution, sediment budgets, sediment modelling and detrital zircon age spectra, the Crockerland terrane is unlikely to have existed as a major sediment supplying area, (3) the reconstructed Arctic sediment routing system can help to constrain plate-tectonic models, and (4) statistical estimation of sediment transport is a novel and potentially important tool for improving plate-tectonic and palaeogeographical reconstructions.

Placement of microcontinents in the Arctic before break-up in the Early Cretaceous is a controversial issue and many different reconstructions have been proposed (e.g. Miller *et al.* 2013, 2018; Shephard *et al.* 2013; Sømme *et al.* 2018; Nikishin *et al.* 2019; Fig. 1). Understanding pre-break-up sediment transport across sedimentary basins in the Arctic could help constrain locations of microcontinents and improve plate-tectonic models, because sediment with known transport routes may serve as 'piercing points' in previously adjacent basins (e.g. Richardson *et al.* 2017). Sediment transport distance and distribution also serves as a holistic sense-check, whereby the basin configuration is considered with a source-to-sink perspective with multi-disciplinary implications for regional tectonics. Enormous sediment volumes were produced in, and prograded from, the Urals and West Siberia in the Carnian and Norian (Late Triassic) across the Greater Barents Sea Basin and Svalbard (GBSB; Klausen *et al.* 2019; Gilmullina *et al.* 2021*b*; Fig. 2). The mapping and budgeting of these deposits offer improved understanding of plate-tectonic process and relative positioning of terranes in the Arctic.

A microcontinent named Crockerland has previously been inferred between the GBSB and the Sverdrup Basin (Fig. 1) based on lithological and facies patterns in these two areas (Mørk *et al.* 1989; Embry 1993). Recent analysis shows that Triassic sediments in the GBSB, including the Late Triassic in Svalbard, are characterized by (1) a large proportion of mudstone, (2) fine- to very fine-grained sandstones (Fig. 3) and (3) a detrital zircon spectrum with a dominant Paleozoic peak and a small number of 'young' zircons close to depositional age (time span between *c.* 210 and 245 Ma; Bue and Andresen 2014; Klausen *et al.* 2015; Fleming *et al.* 2016; Flowerdew *et al.* 2019; Figs 4 and 5), which were supplied from sediment sources in the Urals and West Siberia, rather than Crockerland in the north (Fig. 1; Miller *et al.* 2013; Sømme *et al.* 2018; Gilmullina *et al.* 2021*b*). These sediment properties are similar to those observed in the Late Triassic in the Sverdrup Basin (Embry 1997; Omma *et al.* 2011; Anfinson *et al.* 2016). Furthermore, seismic data (Fig. 2; Gilmullina *et al.* 2021*b*) and sediment volume modelling (Fig. 6) show bypass of large amounts of sediments from the GBSB into adjacent basins (Gilmullina *et al.* 2021*a*). This raises the possibility that sediments previously believed to have originated from Crockerland in fact originated from the Urals and West Siberia and were transported a long distance across mainly subsiding basins.

An understanding of how far the sediments sourced from the Urals and West Siberia could have reached into these adjacent basins is currently lacking. Estimation of the sediment volumes bypassed off the GBSB and size of the potentially receiving basins gives necessary inputs for calculating the length of the system beyond the GBSB.

The goals of this study are fourfold: (1) to present a novel method to determine length of sediment routing systems, developed based on sediment budget calculations and investigation of provenance data; (2) to develop a model that explains Triassic sediment transport in the Arctic; (3) to evaluate whether Crockerland is a necessary concept for the Late Triassic of the Arctic; (4) to discuss how these results compare with existing plate-tectonic reconstructions for the Arctic.
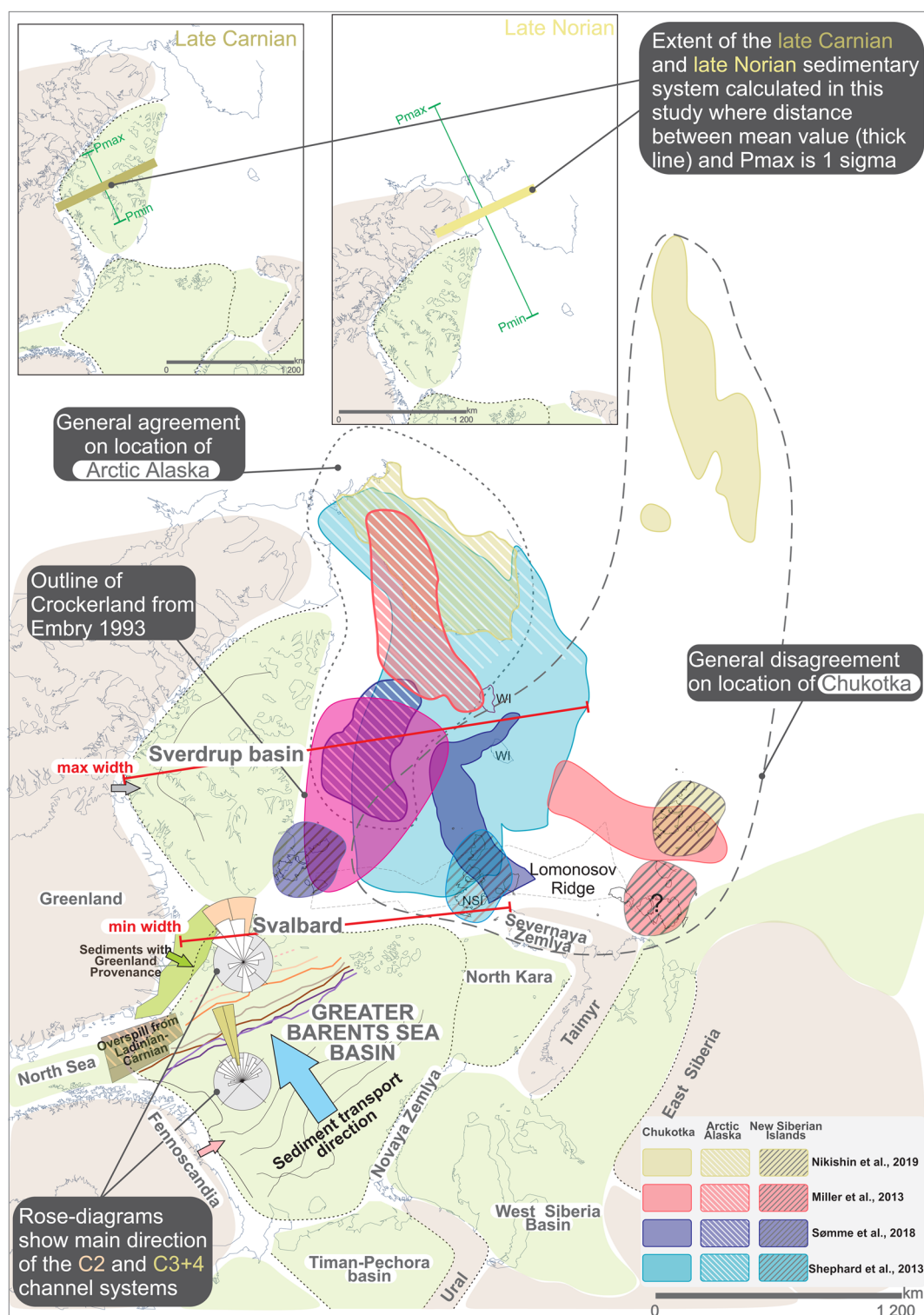
Fig. 1. Overview of the main Triassic sedimentary basins, tectonic elements and sediment source areas referred to in this study and their location during the Triassic. The figure also shows recently proposed locations of the more controversial tectonic elements (Chukotka, Arctic Alaska, New Siberian Islands) and the location of the hypothetical Crockerland landmass. Triassic sediment transport directions in the Greater Barents Sea measured from clinoform belt directions (coloured lines) and fluvial channels (rose diagrams) are also shown, and these data indicate strong NW-directed sediment supply from west Russia to the Barents Sea and beyond. WI, Wrangel Island; NSI, New Siberian Islands.

Triassic Arctic stratigraphy

During the Triassic, the Arctic comprised five main sedimentary basins: the GBSB, Sverdrup Basin, West Chukotka Basin, Arctic Alaska and East Siberian Sea Basin (Fig. 1). Our review of the stratigraphic development in these basins (based on Embry 1997;

Moore *et al.* 2002; Tuchkova *et al.* 2009; Glørstad-Clark *et al.* 2010; Zakharov *et al.* 2010; Klausen *et al.* 2015; Rossi *et al.* 2019; Gilmullina *et al.* 2021*b*) shows that they share a common pattern in sedimentation rates, with large amounts of sediments supplied in the Early Triassic, small amounts in the Middle Triassic and large amounts in the Late Triassic. However, local variations are also evident.
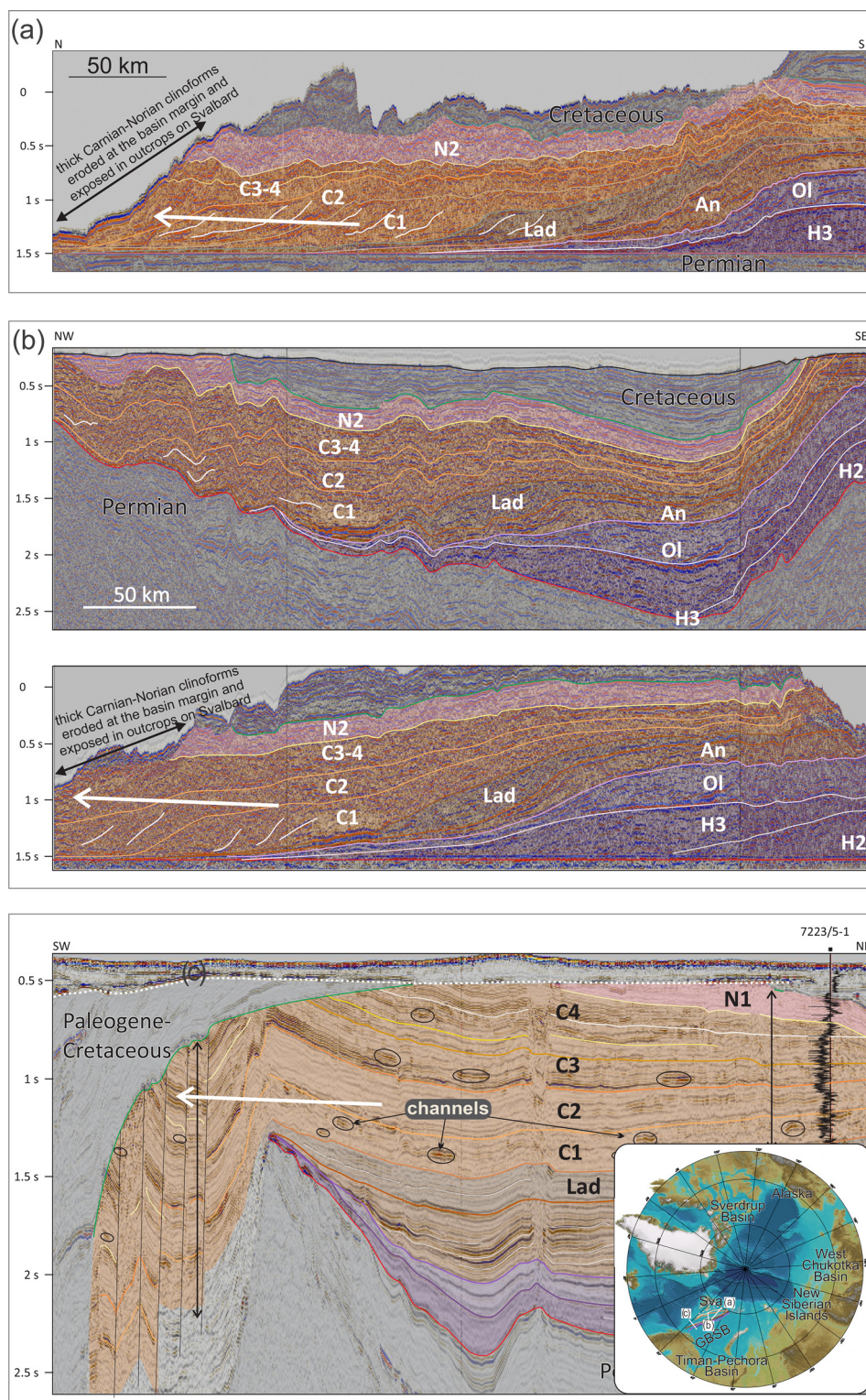
Fig. 2. Interpreted regional 2D seismic data, flattened on the base of Triassic strata, showing the Arctic Barents Sea margin (**a**), the Barents Sea towards Svalbard margin (**b**), and the Atlantic Barents Sea margin (**c**), with a location map of the west Barents Sea showing the line locations. For all these lines, noteworthy features are the large progradational distance of the Carnian section (labelled C1–C4) and late Norian (labelled N2), and that the Carnian is thick but truncated by modern erosion at the margins of the basin, strongly suggesting that the Carnian sedimentary system prograded far beyond the present-day confines of the Greater Barents Sea Basin. The early Norian (labelled N1) unit is transgressive, the late Norian (N2) unit similar to the Carnian (C3 +4) units prograded beyond the GBSB and was later strongly affected by erosion later. The large progradational distance of the Induan (labelled H1–H3) and the comparatively small progradational distance of the Olenekian–Ladinian (labelled Ol, An, Lad) should also be noted.

Greater Barents Sea Basin

The GBSB is filled with up to 4.5 km of sediments, supplied through a linked clinoform–mud-belt–delta–coastal plain system from the Urals and West Siberia termed the Uralo-Siberian source (Klausen *et al.* 2015; Gilmullina *et al.* 2021*b*; Figs 3b and 7). These sediments are represented by a large proportion of mudstone, mineralogically immature and fine-grained sandstones (Bergan and Knarud 1993), late Paleozoic to Triassic detrital zircons (Bue and Andresen 2014; Fleming *et al.* 2016; Klausen *et al.* 2022) and large sediment volumes (Gilmullina *et al.* 2021*a*). Three hundred metres of Late Triassic fluvial deposits are found in outcrops on Svalbard

and Hopen Island (Riis *et al.* 2008; Klausen and Mørk 2014; Lord *et al.* 2014) and confirm a northwesterly sediment transport direction (Klausen and Mørk 2014; Haile *et al.* 2018), indicating that the late Carnian delta system (C3 and C4 units) reached and prograded over the most northwestern part of the GBSB. In the GBSB the early Norian (N1 unit) delta system was transgressed (Klausen *et al.* 2015) and prograded again over Svalbard and the western margin of the GBSB in the late Norian (N2 unit) (Fig. 3b; Klausen *et al.* 2015).

The Uralo-Siberian source had a continental-scale drainage system, able to supply sediment volumes comparable with those at present-day continental margins, which overspilled into adjacent
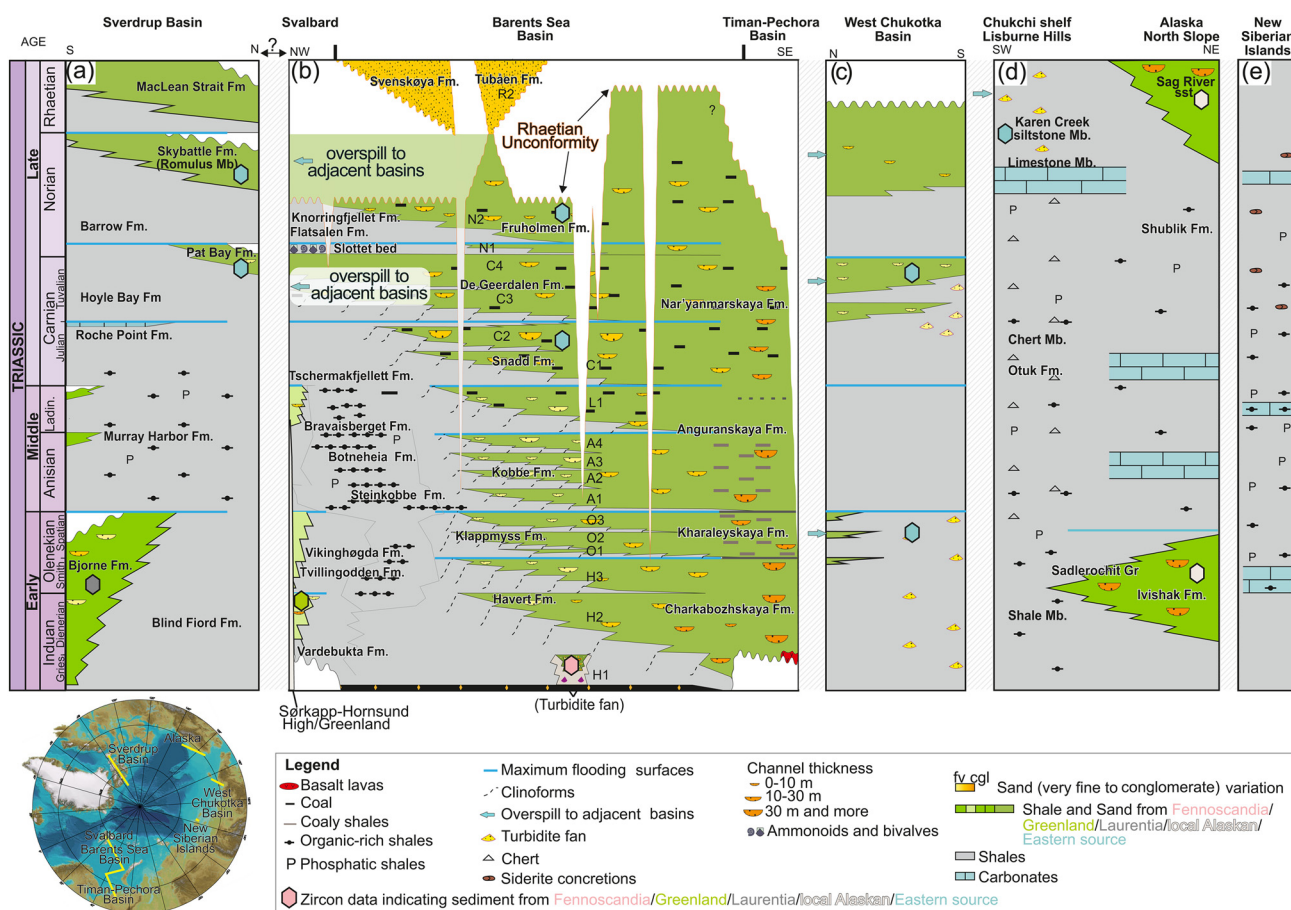
Fig. 3. Compiled lithostratigraphic charts and generalized provenance information of the study area and adjacent sedimentary basins: (**a**) Sverdrup Basin; (**b**) Greater Barents Sea Basin; (**c**) West Chukotka Basin; (**d**) Chukchi Shelf and Alaskan North Slope; (**e**) the New Siberian Islands. A noteworthy feature is the influx of mudstone-rich sedimentary deposits with a typical Uralo-Siberian (eastern) detrital zircon signature in the Early and Late Triassic for West Chukotka, in the Late Triassic for the Sverdrup Basin, and for the Norian on the Chukchi Shelf, indicating a gradual NW-wards progradation of the Uralo-Siberian-sourced sedimentary system in the Late Triassic. Circum-Arctic map from Jakobsson *et al.* (2008).

Arctic basins (Gilmullina *et al.* 2021*a*). Towards the basin margins to Fennoscandia and Greenland, smaller amounts of mature sediments with older detrital zircon age spectra (0.9–2.1 Ma) also occur (Bue and Andresen 2014; Eide *et al.* 2018; Fig. 3b). Organic-rich mudstones of the Steinkobbe and Botneheia formations were deposited in areas so distal they did not receive coarser clastic sediments from the prograding deltas, and were particularly widespread in the Middle Triassic when sediment supply to the basin was smaller (e.g. Krajewski 2008; Krajewski and Weitschat 2015; Gilmullina *et al.* 2021*a*; Fig. 3b).

Sverdrup Basin

The Sverdrup Basin was infilled by deltas, mainly derived from eroded Devonian strata in Arctic Canada, Greenland and local sources (Bjorne Fm) (Fig. 3a), during the Early Triassic (Omma *et al.* 2011; Anfinson *et al.* 2016; Alonso-Torres *et al.* 2018). The Middle Triassic was dominated by dark bituminous shales about 60 m thick (Murray Harbour Fm) (Embry 1997), similar to time-equivalent strata in Svalbard and distal parts of the GBSB (Steinkobbe and Botneheia fms). In the Late Triassic, large amounts of mudstone-rich sediments with very fine- to fine-grained sediments up to 1400 m thick (e.g. the Hoyle Bay, Pat Bay and Skybattle fms, and the Romulus Mbr) were derived from the north, and prograded as shallow-marine to deltaic environments southward across much of the basin (Johannessen and Embry 1989; Embry 1997; Fig. 3a). The traditional view is that these northerly-

derived sediments were supplied from a northern landmass that has been named Crockerland (Fig. 1; Embry 1993). The detrital zircon spectra from these sediments in the Sverdrup Basin were discovered to show the typical Uralo-Siberian source-signature, as also seen in the GBSB (Figs 4a–c and 5), leading to a modification of this hypothesis by its proponents whereby these sediments were transported from the Urals and West Siberia to the Sverdrup Basin through a low-lying but emergent Crockerland (Colpron and Nelson 2011; Anfinson *et al.* 2016; Embry and Beauchamp 2019; Galloway *et al.* 2021). This modified hypothesis still requires the existence of a currently unobservable Arctic landmass. Below, we will make the case that these sediments were not supplied from Crockerland at all but are rather the result of overspill of sediments derived from the Uralo-Siberian source through Svalbard and the northern part of the GBSB.

West Chukotka Basin

Sediments in the West Chukotka Basin were supplied by large delta systems, but the Lower–Middle Triassic deposits were dominated by distal turbiditic, deep-marine continental slope-equivalents to these deltas (Tuchkova *et al.* 2009). During the Carnian, the West Chukotka Basin was dominated by shelf to base-of-slope environments and contains a thick (up to 2 km) package of turbidites, whereas the Norian interval mostly represents a shallow shelf environment, with sediments up to 1 km thick (Tuchkova *et al.* 2009; Fig. 3c).
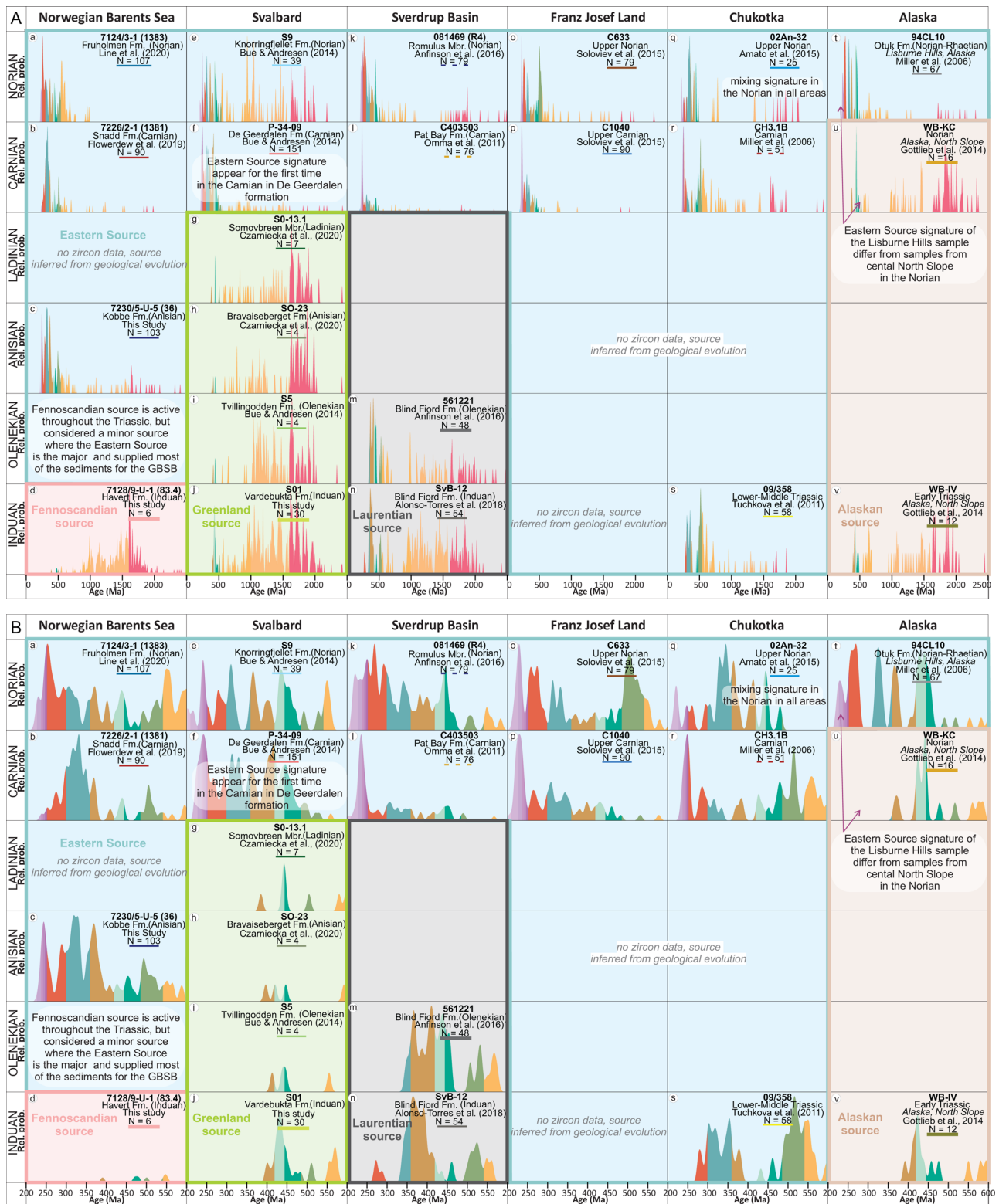
Fig. 4. Compiled published and new detrital zircon age-spectra from the sedimentary systems in the Greater Barents Sea Basin and adjacent arctic basins: (A) $(0–2.5) \times 10^9$ Ma; (B) 200–600 Ma. It should be noted that local detrital zircon signatures (red, green, grey, brown backgrounds) in each of the basin are replaced by the typical Uralo-Siberian signature (blue background) through the Triassic, with replacement happening early in the more proximal areas (GBSB, Chukotka), later in the more distal basins (Svalbard, Sverdrup Basin) and latest in the most distal Alaskan basin. Specta references: Triassic of the GBSB (Flowerdew *et al.* 2019; Line *et al.* 2020), Triassic of Svalbard (Bue and Andresen 2014; Czarniecka *et al.* 2020), Triassic of the Sverdrup Basin (Alonso-Torres *et al.* 2018; Anfinson *et al.* 2016; Omma *et al.* 2011), Triassic of FJL (Soloviev *et al.* 2015), Triassic of Chukotka (Tuchkova *et al.* 2011; Miller *et al.* 2006; Amato *et al.* 2015), Triassic of Arctic Alaska (Gottlieb *et al.* 2014; Miller *et al.* 2006). Sample locations are shown in Figure 5b.

Arctic Alaska

During the Early Triassic, the eastern and central parts of Arctic Alaska were dominated by a fan-delta (Ivishak Fm), which was sourced locally from Laurentia and prograded basinwards to the deep shelf from the north (Houseknecht 2019). The Middle–Upper Triassic is represented by siliciclastic, carbonate and phosphatic deposits of the Shublik Fm with a clastic wedge in its upper part.
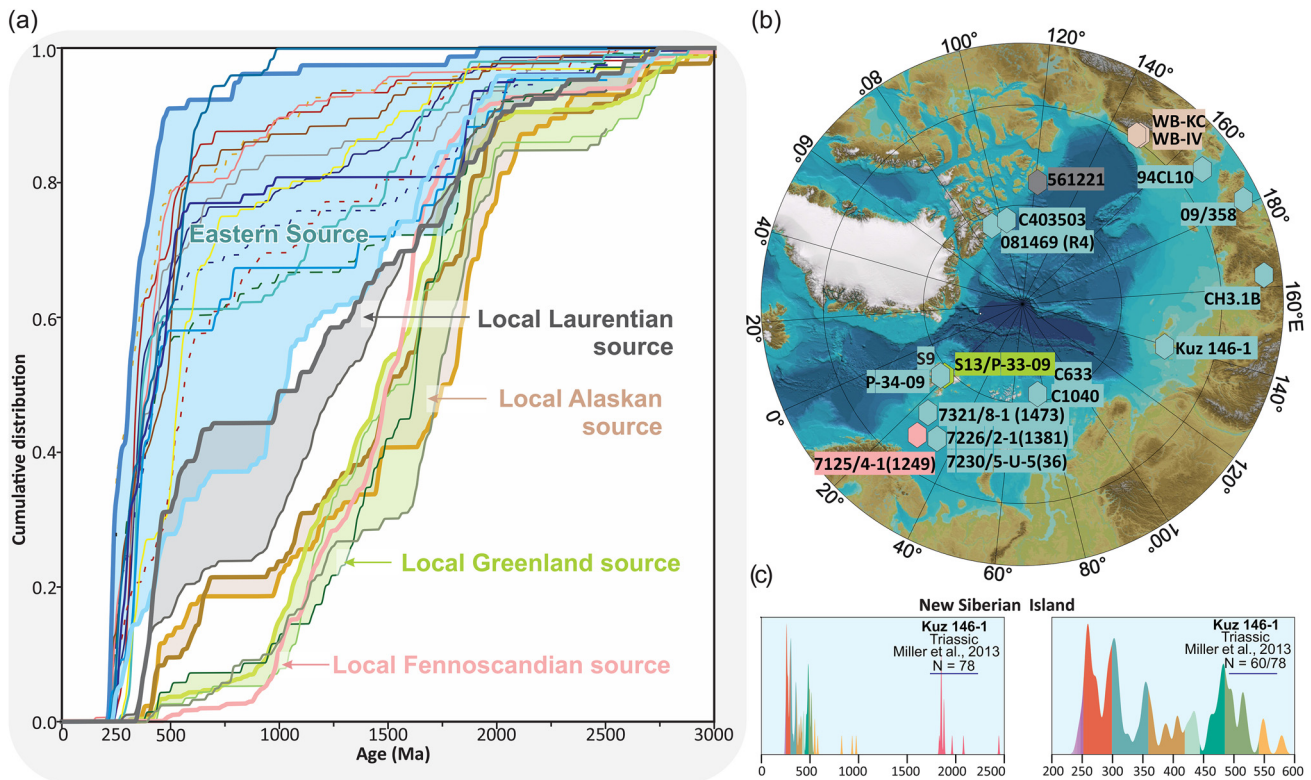
Fig. 5. (**a**) Cumulative detrital zircon age spectra for the various samples in Figure 4, highlighting the difference between the local sources and the eastern source. Colours are the same as the lines bounding the zircon spectra in Figure 4. (**b**) Map showing locations of the samples presented in (**a**) and Figure 4. (**c**) Detrital zircon age-spectra for the New Siberian Island (Miller *et al.* 2013).

This clastic wedge, the Sag River Sandstone, represents a fine-grained marine shelf sourced from Laurentia (or the NE in modern coordinates; Mozley and Hoernle 1990). Throughout the Triassic, western Alaska faced the palaeo-Pacific Ocean and was dominated by an outer shelf environment represented by phosphatic, black shale, chert, and silicified limestone of the Otuk Fm (Tye *et al.* 1999; Moore *et al.* 2002; Houseknecht 2019, Fig. 3d), characteristic of a relatively sediment-starved submarine basin. The Karen Creek Siltstone Mbr in the upper part of the Otuk Fm is, in contrast, represented by very fine- to fine-grained sandstone deposited as turbidites (Moore *et al.* 2002; Whidden *et al.* 2018). The Karen Creek Siltstone Mbr was supplied from the east, possibly from Chukotka, and it is time-equivalent to the Sag River Sandstone (Fig. 3d).

New Siberian Islands

Triassic deposits on the New Siberian Islands are characterized by thin (up to 600 m) shale-dominated deep-water deposits with carbonates, phosphorite and siderite concretions (Egorov *et al.* 1987; Zakharov *et al.* 2010). Detrital zircons of New Siberian Island show great similarity to those from Chukotka Basin samples and suggest that these regions share sediment sources (Miller *et al.* 2013). A clear understanding of the stratigraphic variation through Triassic time is currently lacking owing to complicated tectonic deformation and relatively few studies.

Synthesis of Arctic Triassic stratigraphy

Thus, as shown above, the Arctic basins show two general patterns: (1) the sediment supply is high in the Early Triassic, low and dominated in distal areas by marine productivity during the Middle Triassic, and high again during the Late Triassic; (2) sediments shed from local sources become gradually replaced by

mudstone-rich sediment with a Late Paleozoic and Triassic detrital zircon age peak. This would indicate that these now separated basins were linked prior to break-up, and that sediments were supplied to these basins across significant distances. Whether the sediment budget and catchment characteristics were sufficient to provide enough material to prograde these distances is a key question. Sediment budgets for individual time intervals and their provenance character can tell us whether the progradation length is reasonable and if the sediment source is similar in these areas, and this will be addressed below.

Methods

Dataset

Here we used a database of sediment volumes, stratigraphic seismic interpretations and sediment transport directions based on analysis of 3238 seismic 2D lines, 20 3D seismic datasets, 257 wells and 39 biostratigraphic datings (presented first by Gilmullina *et al.* 2021*b*); a detrital zircon database consisting of two new (DR1) and 16 published samples (Fig. 4); and sediment volumes and sediment supply rates in the GBSB of all stratigraphic units shown on Figure 3b (based on Gilmullina *et al.* 2021*a*).

Sediment volume estimations

Gilmullina *et al.* (2021*a*) estimated sediment volumes supplied to the GBSB per year using two different methods based on (1) observed volumes calculated from the seismic dataset and (2) modelled volumes from the BQART approach involving Monte-Carlo Simulation (MCS). Observed volumes calculations are based on (1) estimation of the time–thickness of each stratigraphic time unit, determined by interpreting the available dataset described above, (2) depth-conversion of top and bottom surfaces of each time unit, (3) calculation of the mass of each unit by multiplying
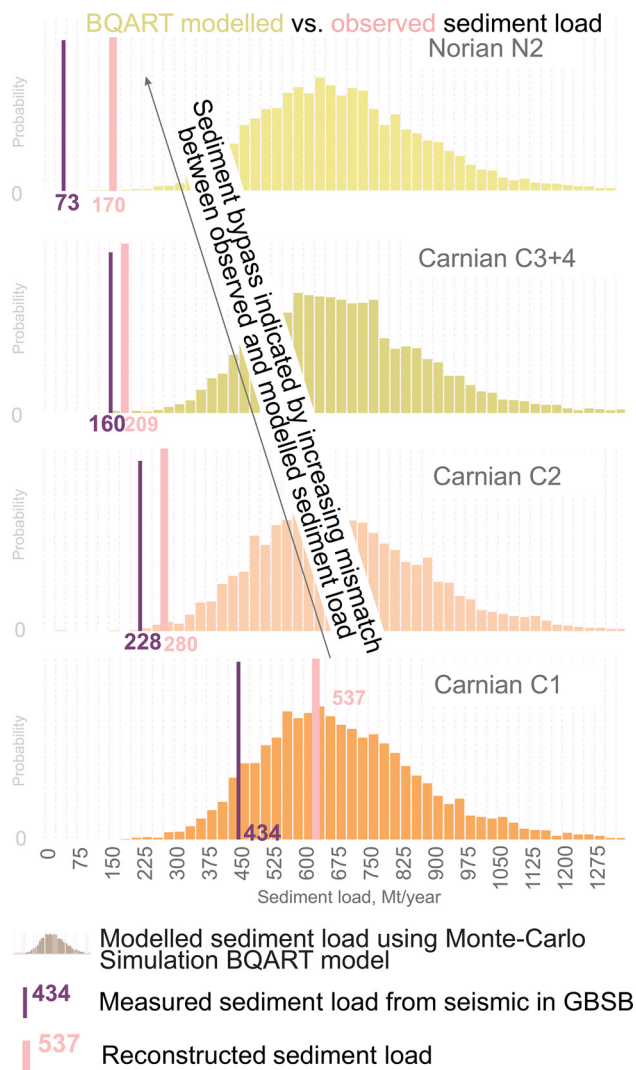
Fig. 6. Probability distributions for modelled sediment supply from the Uralo-Siberian sediment source to the GBSB for the investigated Carnian and Norian time periods, and how these models relate to observed (where erosion is not accounted for) and reconstructed (erosion accounted for) sediment supply to the GBSB. It should be noted that for the C1 interval, when the clinoforms did not prograde beyond the GBSB, the modelled and reconstructed sediment supply matches. For the later time steps, there is a progressive mismatch between modelled and observed sediment load, indicating that progressively larger amounts of sediment bypassed from the GBSB to adjacent basins. Distributions shown are after Gilmullina et al. (2021a).

thickness maps by density maps, created based on density logs from available wells, and (4) division of mass of each time unit by duration determined by biostratigraphic data.

Modelled volumes are based on the empirical BQART model created by Syvitski and Milliman (2007). The model depends on input variables and shows the sediment load from the catchments that supplied sediments to the sink, described by equation (1):

$$Q_s = \omega L Q_w^{0.31} A^{0.5} RT \tag{1}$$

where Q_s is sediment discharge (10^6 t a^{-1}), ω is an empirical constant ($\omega = 0.0006$), L is a variable for bedrock erodibility (with extremes of 0.5 to three for hard metamorphic–plutonic bedrock lithologies and erodible loess lithology, respectively), Q_w is annual water discharge (km^3 a^{-1}), A is catchment area (km^2), R is maximum catchment relief (km), and T is the long-term basin-averaged temperature (°C). Gilmullina et al. (2021a) used MCS to model sediment supply based on realistic catchment parameters described above. Each input parameter was assigned to a normal distribution within limits, and the MCS performed 10 000 realizations per stratigraphic unit. The methods have been explained in detail by Gilmullina et al. (2021a).

In this paper we use the sediment load calculated for the Late Triassic, and input parameters for the BQART MCS are described below.

The lithology parameter (L) was assigned a normal distribution with a range between 0.75 and 1.5 and an overall average value of unity, estimated for a catchment area with a wide variety of clastic, igneous and metamorphic lithologies (Petrov et al. 2012, 2016; https://vsegei.ru/ru/info/webmapget/).

Temperature values (T) were assigned to a normal distribution between 0 and 12°C, associated with cooler and more humid climate after greenhouse dominated in the Early Triassic (Scotese and Moore 2014).

The catchment area (A) for the Late Triassic includes a vast area of the Uralo-Siberian source, including the West Siberia Basin with the western part of the Siberian Platform, northern Central Asian Orogenic Belt in the south, Taimyr in the north and the Novaya Zemlya Fold and Thrust Belt, supported by detrital zircon studies (Omma 2009; Tevelev 2013; Bue and Andresen 2014; Soloviev et al. 2015; Fleming et al. 2016; Flowerdew et al. 2019; Khudoley et al. 2019; Klausen et al. 2017, 2019), and quartz fluid inclusions (Haile et al. 2021). Separate normal distributions were assigned for each sub-catchment within the overall catchment area. The maximum catchment relief parameter (R) was assigned to a normal distribution according to sub-catchments and was based on a general understanding of tectonic evolution and modern relief analogues: the Urals 2–6 km, the Central Asian Orogenic Belt 3.5–7 km, the West Siberia Basin 0.5–1.5 km and the Taimyr 0.5–9 km.

Detrital zircon age analysis

Here, we present new detrital zircon U/Pb ages from two samples: one outcrop sample from the Induan Vardebukta Fm in the Festningen section on Svalbard (Fig. 4j), and one sample from
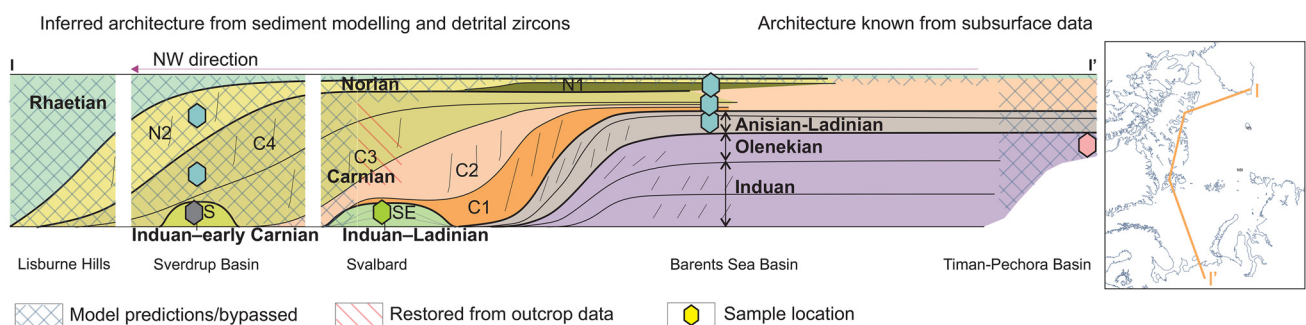

Fig. 7. Schematic distribution of sedimentary architecture in the Arctic basins, and the relationship between observed sediments in the GBSB and on Svalbard assumed bypassed sediments to basins beyond.

the Induan Havert Fm from a cored stratigraphic borehole on the Finnmark Platform (well 7128/9-U-1 at 83.40 m depth, Fig. 4d). The drill core sample was made available by the Norwegian Petroleum Directorate (NPD).

The samples were crushed with a disc-mill, before the zircons were concentrated, using panning and density separation techniques. Instead of hand-picking, the zircons were extracted for mounting by pipetting of ethanol to limit bias during picking. The zircons were then embedded in epoxy, ground to about half the grain thickness and polished to expose the grain cores. The grain mounts were further photographed with backscatter and cathodoluminescence detectors, using a Zeiss Supra 55VP scanning electron microscope, prior to laser ablation inductively coupled plasma mass spectrometry (LA-ICP-MS) analyses at Bergen Geoanalytical Facility, University of Bergen.

For each sample, 331–349 zircons were analysed by a Nu AttoM high-resolution ICP-MS system, coupled to a 193 nm ArF excimer laser (Resonetics RESOlution M-50 LR). The laser was fired at a repetition rate of 5 Hz and with an energy of 90 mJ, using a spot size of 26 μm. Typical acquisitions consisted of 15 s measurement of blank, followed by 30 s of measurement of U, Th and Pb signals from the ablated zircon. The data were acquired in time resolved–peak jumping–pulse counting mode with one point measured per peak for masses $^{204}Pb + Hg$, ^{206}Pb, ^{207}Pb, ^{208}Pb, ^{232}Th, ^{235}U and ^{238}U. The raw data were preprocessed using a purpose-made Excel macro because of a nonlinear transition between the counting and attenuated (= analogue) acquisition modes of the ICP instruments. As a result, the intensities of ^{238}U were left unchanged if measured in a counting mode and recalculated from ^{235}U intensities if the ^{238}U was acquired in an attenuated mode. The data reduction (correction for gas blank, laser-induced elemental fractionation of Pb and U, and instrument mass bias) was carried out off-line using the Iolite data reduction package (v. 3.0), with VizualAge utility (Petrus and Kamber 2012). Details of the data reduction method have been given by Paton *et al.* (2010). For the data presented here, blank intensities and instrumental bias were interpolated using an automatic spline function, and down-hole interelement fractionation was corrected using an exponential function. No common Pb correction was applied to the data, but the low concentrations of common Pb were controlled by observing the $^{206}Pb/^{204}Pb$ ratio during measurements. Residual elemental fractionation and instrumental mass bias were corrected by normalization to the natural zircon reference material 91500 (1065 Ma: Wiedenbeck *et al.* 1995). Zircon reference materials GJ-1 (609 Ma: Jackson *et al.* 2004) and Plešovice (337 Ma: Sláma *et al.* 2008) were periodically analysed during the measurement for quality control. The GJ-1 and Plešovice standards provided ages of 599.2 ± 0.4 Ma and 345.2 ± 0.3 Ma, respectively, when calibrated against the 91500 standards.

To compare previously published datasets with the new data, all analyses have been filtered in a similar way. The data have been filtered for discordance >10% or <−10% and relative error on age <20% (2σ). For the new data, 66 out of 680 analyses were rejected. The detrital zircon data are visualized and analysed by the Python-based detrital Py-package (Sharman *et al.* 2018). For grains <1000 Ma, the $^{238}U/^{206}Pb$ age was used, whereas the $^{207}Pb/^{206}Pb$ age was used for the older grains. Uncertainties are given at 2σ confidence level.

Modelling Triassic sediment input and distribution

As indicated above, we have used a novel approach to reconstruct the distribution and the length of the easterly derived Triassic sediment beyond the GBSB, which was developed based on sediment budget calculations.

The well-established BQART approach (Syvitski and Milliman 2007; Sømme *et al.* 2013; Zhang *et al.* 2018; Brewer *et al.* 2020;

Nyberg *et al.* 2021), can provide an estimate of sediment supply (in mass per time) to sedimentary basins when a series of key parameters about the catchment are provided (lithology, relief, area, temperature, degree of glacial coverage and water discharge). Gilmullina *et al.* (2021a) compared the sediment load to the GBSB measured from the seismic data with what could be expected to have been delivered from the Uralo-Siberian source throughout the Triassic using a BQART–MCS approach to quantify and represent the uncertainty for the unknown input values. Their results showed that there was generally an excellent fit with the estimated sediment load of the sedimentary units that were fully constrained within the seismic data (Induan, Olenekian and Carnian C1). Sediment loads in late Carnian (Carnian C2, Carnian C3 + 4), and Norian (Norian N2) units, as determined from seismic data, are all towards the lower end of the modelled sediment loads, constituting 40, 30 and 25% of the mode of the modelled sediment loads, respectively (Fig. 6). This indicates loss of a significant amount of sediment from the GBSB, and large-scale sediment bypass beyond the present-day limits of the GBSB can explain the documented similarities of the Upper Triassic sediments in other Arctic basins.

We assume that the difference between averages of modelled sediment loads and observed sediment loads approximate the amount of sediment that prograded over from the GBSB into adjacent sedimentary basins. The minimum width of the Arctic Basin was estimated as the distance between Svalbard and the Severnaya Zemlya Archipelago, essentially the area with confirmed distribution of the Triassic sediments (Shneyder *et al.* 1989). The maximum width of the circum-Arctic basinal areas was based on the 200 Ma reconstruction of Shephard *et al.* (2013). We used an average basin depth of 500 m as many of the backstripped second-order clinoform surfaces in the GBSB scale to such depths (Klausen and Helland-Hansen 2018), and the thickness of late Triassic formations seems to have scaled to such thicknesses before post-depositional erosion (Klausen *et al.* 2017). Thicknesses of the second-order Carnian and Norian sequences in the Sverdrup Basin are accordingly *c.* 300 and 400 m (Embry 2011).

Estimation of the sedimentary system's progradation length was made by the following workflow: (1) the volume of missing sediments per unit was calculated as a difference between modelled values that lay within the centre of the normal distribution and observed sediment load and (2) divided by the mean basin depth and (3) basin width (Table 1). This leads to a depositional model for the Arctic, which is independently verified using published and new (DR1) detrital zircon age data (Fig. 4).

Results

Estimation of bypassed sediment volumes from GBSB

The BQART model shows that the Uralo-Siberian source had potential to generate 670 (±190) MT of sediments per million years in the Carnian (Gilmullina *et al.* 2021a). During the Triassic until the early Carnian, sediments from the Uralo-Siberian source were largely contained within the GBSB, but after this sedimentary geometries show that progressively greater amounts of sediments prograded from the GBSB to basins to the north (Figs 1–3). This is also seen as a progressively increasing mismatch between sediment load observed in seismic data and modelled sediment load (Fig. 5, Table 1). Assuming constant sediment production in the catchment through the Carnian, which seems reasonable based on the uniform clinoform thickness and relief, 6.7×10^9 MT of sediments were produced in the Uralo-Siberian source, and *c.* 60% of these sediments bypassed to basins to the north and NW of the GBSB (DR2).

Norian strata in the GBSB are strongly eroded, especially towards the Finnmark Platform, Loppa High and Svalbard, but also locally

Table 1. *Main inputs for calculation of possible distance that the Late Triassic prograded beyond the GBSB modern boundaries*

Unit	Seismic (Mt a⁻¹)	MCS BQART (Mt a⁻¹)			Missing (Mt a⁻¹)	Age/duration (years)	Density (t km⁻³)	Volume (km³)		Basin width (km)		Basin depth (km)	Distance	
		Mean	Median	1σ				Per year	Total	Minimum	Maximum		km	1σ
C3 + 4	252	670	650	190	666	6000000	2.5×10^9	0.1744	1046400	1400	2600	0.5	1000	500
N2	170	670	660	190	600	18500000	2.5×10^9	0.2072	3833200	1400	2600	0.5	3700	1500

around salt domes reactivated at the Triassic–Jurassic transition (Müller *et al.* 2019). Estimates of Norian sediment supply are, therefore, more uncertain than those for the Carnian. If the Uralo-Siberian source continued to generate the same amounts of sediments, 12.4×10^9 MT were generated. *c.* 25% of these sediments in the GBSB were later eroded and 65% probably bypassed to basins beyond.

How far did bypassing sediments prograde into the Arctic basins?

Using the sediment volumes calculated above, it is possible to estimate how far the sediments that bypassed the GBSB prograded into the adjacent basins. Basin geometry is approximated using a simple rectangular prism, where the width is assigned to normal distribution between a minimum and maximum distance equal to the distance between Svalbard and Severnaya Zemlya of 1400 km and circum-Arctic reconstruction by Shephard *et al.* (2013) of 2600 km. Prism height equals average basin depth, approximated by the decompacted sediment thicknesses in the Sverdrup Basin. Average thicknesses of Late Triassic deposits in the Sverdrup Basin are up to *c.* 310 m, which translates to thicknesses of 560 m (DR2) when applying similar decompaction parameters and method, as used in a study on time-equivalent strata in the Barents Sea by Klausen and Helland-Hansen (2018).

Using this simple model, the mean progradation lengths of bypassed sediments beyond the GBSB become 1000 (±500) km for the Carnian and 3300 (±1300) km for the Norian (DR2) (Figs 1a and 7). This implies that sediments from the Uralo-Siberian source, bypassing the GBSB, could have supplied sediment through nearly the entire Sverdrup Basin in the Carnian, and all the way to Arctic Alaska in the Norian.

Are these progradation lengths supported by detrital zircon data?

The calculated progradation lengths are supported by a compilation of new and previously published detrital zircon age data in the Arctic basins throughout the Triassic (Figs 4 and 5). These data show that most areas were initially dominated by locally derived sediments. In the Southern Barents Sea (Lower Triassic), the local source is dominated by Paleoproterozoic–Early Neoproterozoic detrital zircon ages, typical for a Fennoscandian sediment source (Figs 4d and 8–12; Eide *et al.* 2018). On Svalbard, the local source is documented in the Lower–Middle Triassic sections (Fig. 4g–j; Bue and Andresen 2014). Although there are similarities to the typical Fennoscandian age signature, these age distributions additionally include a more prominent early–middle Paleozoic age component, which indicates a Greenland sediment source. Lower Triassic samples from the Sverdrup Basin (Anfinson *et al.* 2016; Alonso-Torres *et al.* 2018) are mostly characterized by Proterozoic and early–middle Paleozoic detrital zircon ages (Fig. 4m and n). Also, a small *c.* 290–250 Ma age peak indicates a short-lived, local magmatic event that occurred in the Sverdrup Basin during the Permian (Omma 2009; Omma *et al.* 2011; Gottlieb *et al.* 2014; Anfinson *et al.* 2016; Hadlari *et al.* 2016; Midwinter *et al.* 2016; Alonso-Torres *et al.* 2018). These age distributions are typical for a Laurentian sediment source in the Sverdrup Basin. The local sources recorded in the Southern Barents Sea, Svalbard and Sverdrup Basin remained dominant until the prograding Uralo-Siberian sedimentary system arrived at different times in different locations.

The Uralo-Siberian sediment source is typically characterized by a group of *c.* 200–250 Ma zircons (*c.* 20–30%), a dominant population of *c.* 250–370 Ma zircons (*c.* 50%) and smaller groups of zircons with ages of *c.* 390–500 Ma and *c.* 540–620 Ma. Scattered
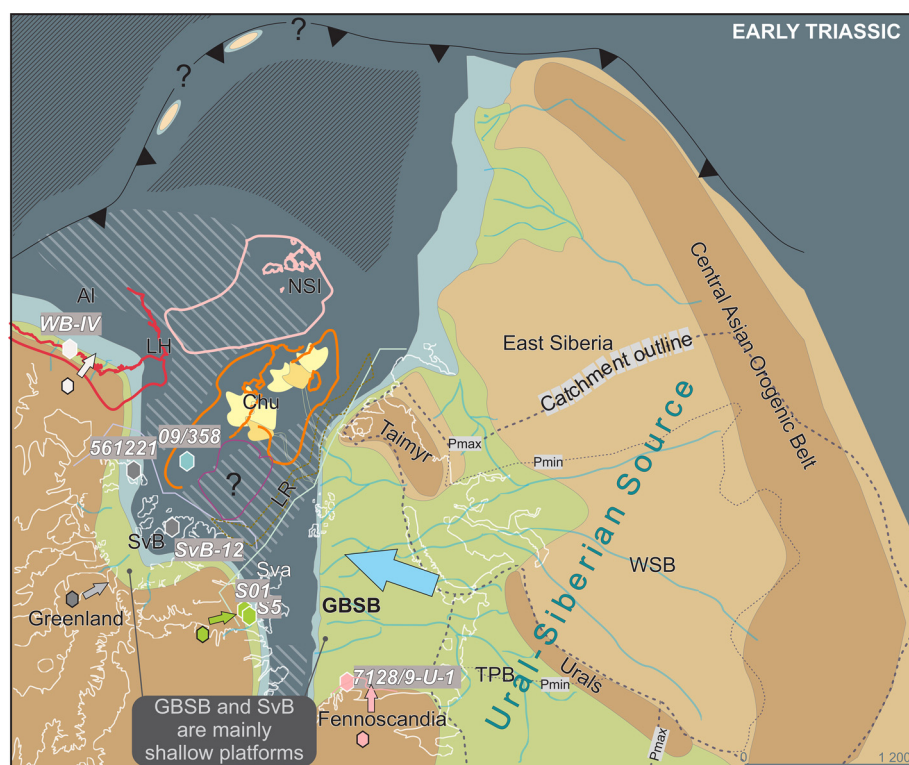
Fig. 8. Palaeogeographical map of the Arctic and surrounding regions during the Early Triassic. This time period was characterized by extremely high terrigenous sediment supply and active local sources in several of the Arctic basins. Legend is given in Figure 12. TPB, Timan-Pechora Basin; WSB, West Siberia Basin, other abbreviations are as in Figure 13.

older ages can also occur in minor amounts (Figs 4a–c and 8; Fleming *et al.* 2016; Klausen *et al.* 2017; Flowerdew *et al.* 2019). However, there is a change from the early to the late Carnian, where the abundance of zircons younger than *c.* 250 Ma strongly increases (Omma 2009; Bue and Andresen 2014; Fleming *et al.* 2016; Klausen *et al.* 2022). Unfortunately, too few detrital zircons age spectra have been published from the relevant areas, especially the Northern Urals Foreland Basin and South Kara. It is, therefore, difficult to say whether this change is caused by (1) increased magmatic activity in the West Siberia and Central Asian Orogenic Belt, (2) onset of magmatic activity in the Novaya Zemlya Fold and Thrust Belt or (3) a combination of these. The exhumation of Novaya Zemlya probably occurred during the Carnian (Klausen *et al.* 2014; Gilmullina *et al.* 2021a), and the possibility that it acted as a barrier for sediments coming from West Siberia could not be excluded. However, detrital zircon age signatures for Triassic samples from the Moscow Basin (Western Urals Catchment) do not include any Triassic zircons (Chistyakova *et al.* 2020), and it is therefore likely that the young zircons were derived from West Siberia or Novaya Zemlya, or a combination of these.
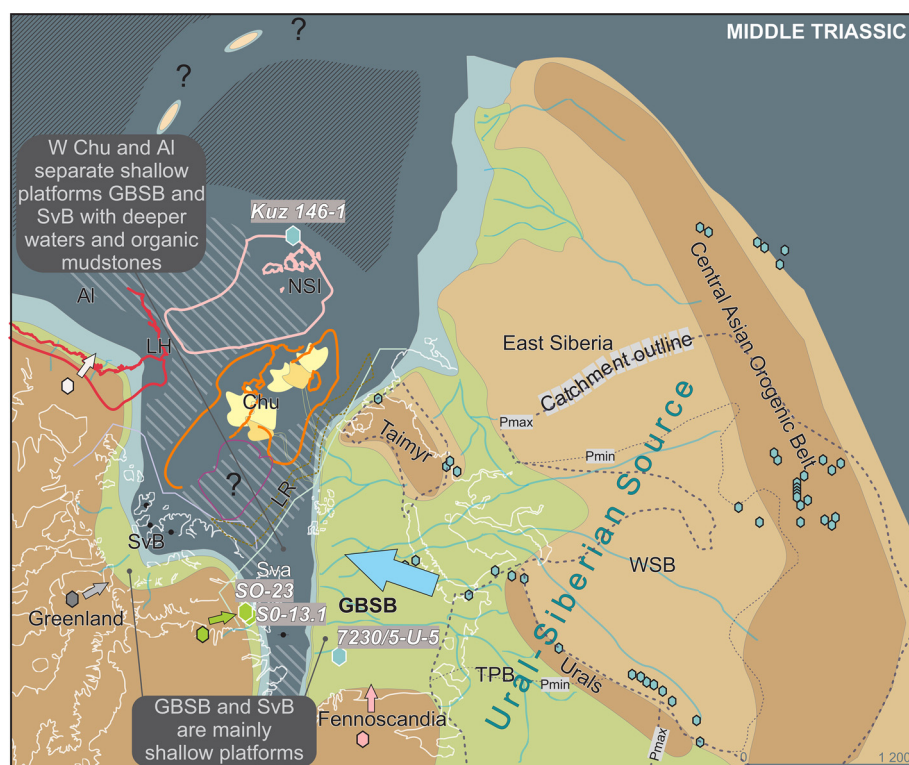

Fig. 9. Palaeogeographical map of the Arctic and surrounding regions during the Middle Triassic. This time period was characterized by relatively low terrigenous sediment supply and upwelling-related deposition of phosphatic, organic-rich mudstones in several of the Arctic basins. Legend is given in Figure 12. Abbreviations are as in Figure 13.
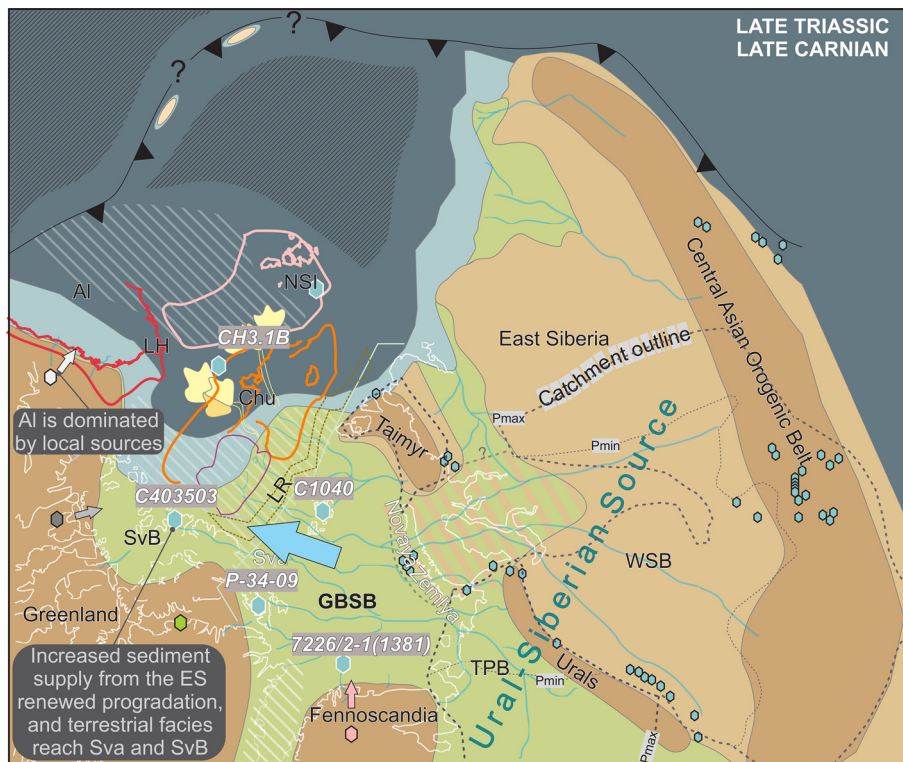
Fig. 10. Palaeogeographical map of the Arctic and surrounding regions during the Late Triassic Carnian stage. This time period was characterized by very high terrigenous sediment supply from the Polar Urals and incipient uplift of Novaya Zemlya. The progradation of typical Uralo-Siberian sediments into the Sverdrup Basin and progradation from sandy deep-marine fans to shallow-marine deposits in Chukotka was probably a result of this sediment supply. Alaska is dominated by local sources at this time, indicating that the Uralo-Siberian system did not reach this far. Legend is given in Figure 12. Abbreviations are as in Figure 13.

In areas close to the Uralo-Siberian source, such as the Finnmark Platform (Figs 1, 4d and 8), locally derived sediments were already replaced by sediments from the Uralo-Siberian source in the Induan (Early Triassic). The Uralo-Siberian source-signature is characteristic of the succession in Chukotka throughout the Triassic, indicating that it was located close to this provenance throughout the Triassic. In medial areas, such as Svalbard, locally derived sediments persist until sediments from the Uralo-Siberian source arrive in the earliest Carnian (C1, Figs 3 and 4e, f). At the GBSB,

Svalbard, Chukotka and Sverdrup Basin (Fig. 1), an incursion of a mudstone-rich sedimentary system with sparse fine-grained sandstones with a typical Uralo-Siberian source detrital zircon signature occurs in the Late Carnian (Figs 4j, k and 9). In Arctic Alaska, locally derived zircon age spectra are observed in the Norian (Figs 4s, 8 and 9), but the characteristic young Uralo-Siberian source-signature becomes mixed in with the local signal in the late Norian (Figs 4r and 10) suggesting that the system reached all the way to Arctic Alaska. This distribution of detrital zircon ages fits well with
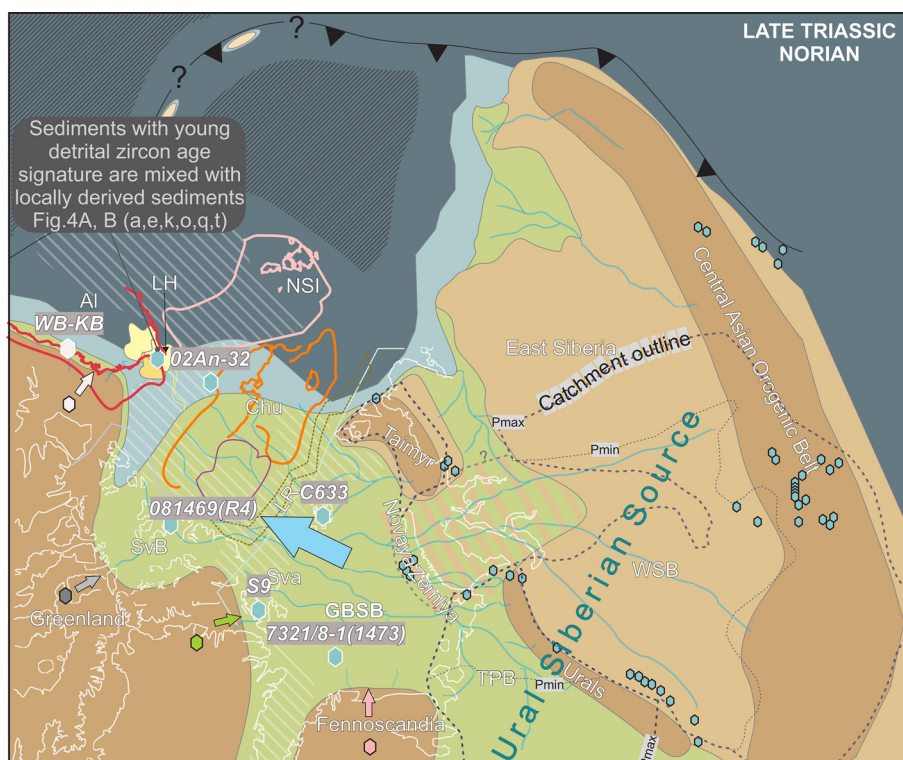

Fig. 11. Palaeogeographical map of the Arctic and surrounding regions during the Late Triassic Norian stage. This time period was also characterized by very high terrigenous sediment supply from the Polar Urals and incipient uplift of Novaya Zemlya. This time period records the largest extent of terrestrial and shallow-marine sediments with an Uralo-Siberian signature, and turbiditic sandstones in Lisburne Hills show the typical detrital zircon signature during this time. Significant terrigenous deposits have not been recorded on the New Siberian Islands. Legend is given in Figure 12. Abbreviations are as in Figure 13.
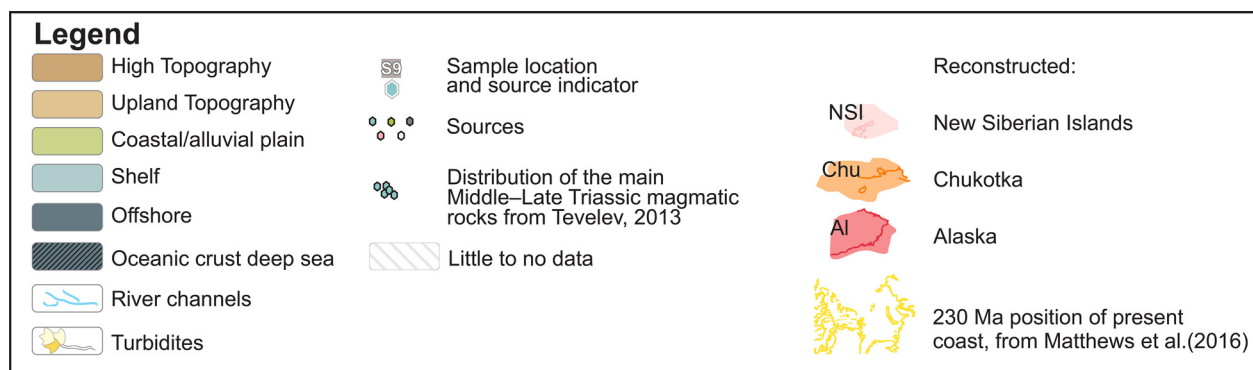
Fig. 12. Legend for Figures 8–11, coastline from Matthews *et al.* 2016.

calculated progradation lengths of bypassed Uralo-Siberian source sediment for each unit prograding sequentially from the GBSB (Fig. 1).

Discussion

Implications for plate-tectonic reconstructions

Looking at the current basin structure in the Arctic, the youngest ocean basin is the early Cenozoic to Recent Eurasia Basin (Fig. 13). Before this basin opened, the Lomonosov Ridge is by all researchers

reconstructed at the edge of the Barents Shelf. The earlier phase of opening formed the Amerasia Basin in the Cretaceous, but the lack of magnetic anomalies (Gaina *et al.* 2011; Zhang *et al.* 2019) and lack of good understanding of the kinematics of the opening make it difficult to choose one unique palaeogeographical model for the structure of the Arctic prior to rifting. This is where the model for sediment dispersal presented above has important implications for plate-tectonic reconstructions in the Arctic.

The sedimentary record of the Chukotka Basin follows the same sediment supply trend and contains late Paleozoic and Triassic zircons best explained by bypass from a Uralo-Siberian source
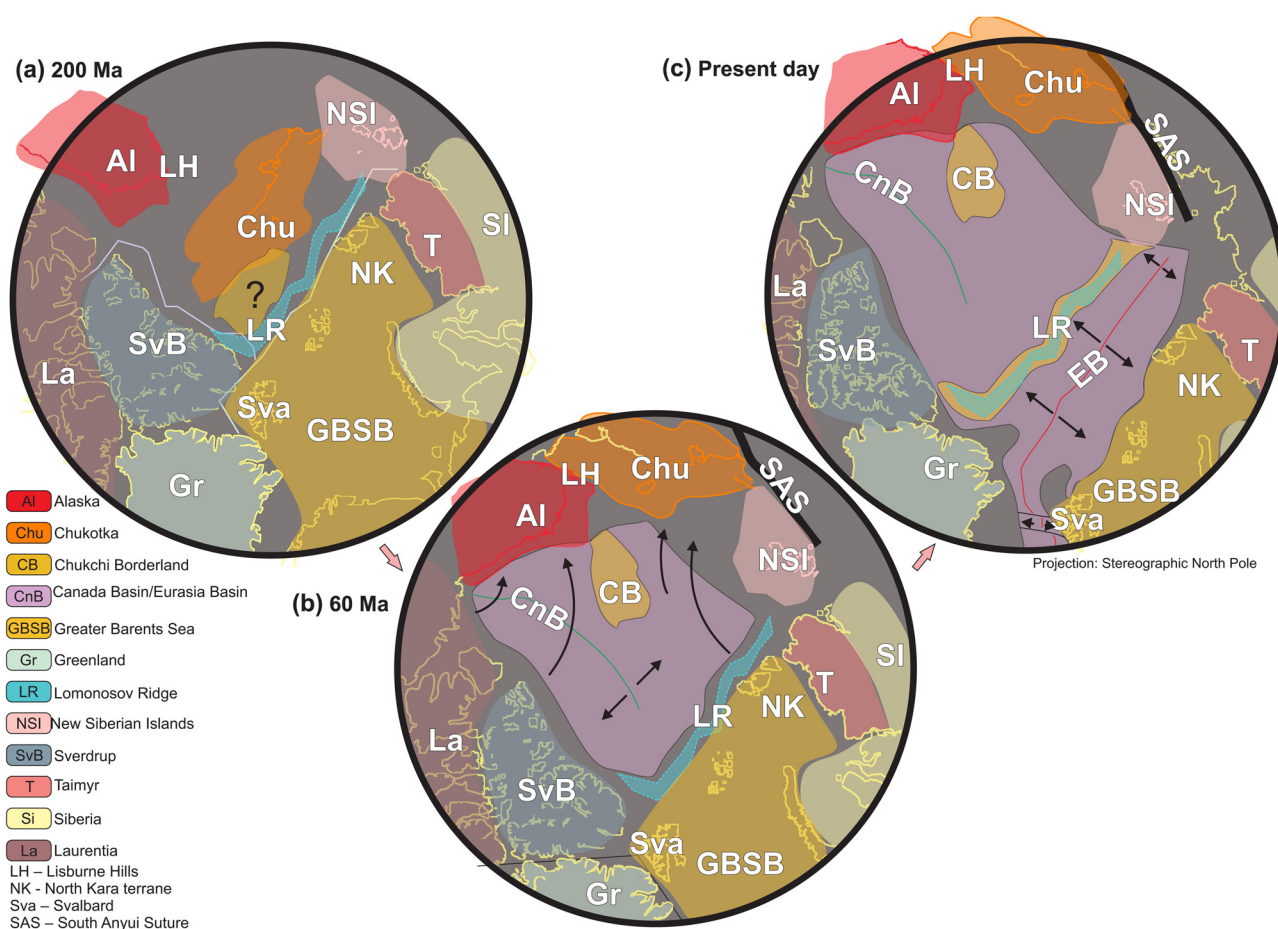

Fig. 13. Suggested palaeogeographical reconstructions based on the constraints provided by the sedimentary evidence presented herein. (**a**) Most likely pre-break-up setting at the end of the Triassic. The sedimentary evidence requires a distal position of the New Siberian Islands, a close docking of the GBSB, Chukchi Borderland and Chukotka; and a position of the Chukotka Basin and Arctic Alaska near Laurentia. (**b**) Opening of the Amerasia Basin, where Alaska and Chukotka rotate counter-clockwise away from Laurentia (from Doré *et al.* 2016). (**c**) Opening of the Eurasia basin, in which the Lomonosov Ridge is rifted off and drifts away from the northern margin of the GBSB, with transform motion distancing the previously adjacent Sverdrup Basin and GBSB.

throughout the Triassic (Figs 8–12). This implies a close docking of the Lomonosov Ridge against the northern GBSB, and Chukotka docked close to the Lomonosov Ridge, as suggested by Miller *et al.* (2013, 2018; Fig. 1a). Chukotka is then located closer to the GBSB (different from Nikishin *et al.* 2019) and rotated more than in the reconstruction of Shephard *et al.* (2013) and Sømme *et al.* (2018) (Fig. 13). The GBSB and Greenland blocks were in that case located very close to the Sverdrup Basin (Fig. 13).

The East Siberian Sea shelf, including New Siberian Islands (NSI), is one of the most complex and poorly understood areas in the Arctic (Piepjohn *et al.* 2018; Prokopiev *et al.* 2018). The pre-break-up location of the NSI and its affiliation to Arctic or Siberia is disputed (Kuzmichev 2009; Ershova *et al.* 2015). The NSI deposits represented the deepest and most distal facies of the Uralo-Siberian system throughout the Triassic (Figs 8–12; Egorov *et al.* 1987; Zakharov *et al.* 2010). Thus, a position of the NSI adjacent to the Sverdrup Basin or Severnaya Zemlya and the GBSB is unlikely because these areas are dominated by fluvial deposits in the Carnian and late Norian (Figs 9–11). Only very distal facies, mainly thinly bedded shales with carbonate interbeds, are present during these times in the NSI. To deposit such distal deposits and still contain zircons with a Uralian signature, the location of the NSI must have been far offset from the main sediment transportation route, in more distal locations in line with suggestions made by Nikishin *et al.* (2019; Fig. 1). The precise Triassic location of the NSI remains to be resolved and is an interesting topic for future study.

A location of Arctic Alaska near Laurentia (Miller *et al.* 2013; Shephard *et al.* 2013; Nikishin *et al.* 2019; Døssing *et al.* 2020; McClelland *et al.* 2021) is the least controversial among reconstructed terranes; however, the angle of rotation of the continent, associated with Amerasia Basin opening, is very different depending on the researcher (Fig. 1). Distribution of sedimentary environments and published detrital zircon data support a rotation of Arctic Alaska as suggested by Shephard *et al.* (2013) and Gottlieb *et al.* (2014). Such a rotation is in accordance with the fact that sediments with an Uralo-Siberian source-signature are found only in the Lisburne Hills in the SW part of Arctic Alaska (Figs 4t and 10).

During the Carnian–Norian, the Arctic basins (GBSB, Sverdrup, Chukotka, New Siberian Island, Wrangel Island, Alaska) received clastic sediments with a significant group of zircons with ages close to the depositional age (Fig. 4; Miller *et al.* 2013; Flowerdew *et al.* 2019). Many studies have discussed the origin of these zircons and suggested different potential sources such as Taimyr (Omma *et al.* 2011; Fleming *et al.* 2016), the 'Pangean Rim of Fire' or a subduction zone along the western margin of Laurentia (Hadlari *et al.* 2017). Our results also imply that the presence of these 'young' zircons in the Upper Triassic deposits do not argue in favour of a magmatic arc system (e.g. Midwinter *et al.* 2016; Hadlari *et al.* 2017) extending all the way into the Arctic region. This is because similar zircon age populations were produced by the Uralo-Siberian source (Figs 8–12; Tevelev 2013; Klausen *et al.* 2017; Gilmullina *et al.* 2021a), and because sedimentary systems sourced from the Urals and Siberia, and prograding northwestwards across the GBSB into the wider Arctic, are the most likely prime cause of the Triassic zircon distribution.

Is Crockerland a necessary concept in the Triassic?

The Crockerland terrane is a hypothetical landmass proposed to explain the facies distribution in Svalbard and the Sverdrup Basin (Fig. 1; Embry 1993). There are, however, numerous problems with this suggestion. First, clinoforms in the GBSB show sediment transport towards the NW (Riis *et al.* 2008; Glørstad-Clark *et al.* 2010; Gilmullina *et al.* 2021b) and Late Triassic channels in the GBSB and Svalbard also show sediment transport towards the NW (Klausen and Mørk 2014; Haile *et al.* 2018), which implies that

sediment was transported from the Uralo-Siberian source across the Barents Sea over Svalbard throughout the Late Triassic in a direction trending directly towards where the Sverdrup Basin was located (Miller *et al.* 2013; Gilmullina *et al.* 2021b). The deep basin that was situated between the Uralo-Siberian source and Laurentia–Greenland accommodated thick, organic-rich marine shales of the Middle Triassic Steinkobbe, Botneheia and Murray Harbor formations, until the basin was finally filled in the Late Triassic. Previous studies have inferred a land bridge across the Arctic, merging with the proposed Crockerland landmass to explain Uralo-Siberian detrital zircons in the Sverdrup Basin (Anfinson *et al.* 2016; Sømme *et al.* 2018). This explanation implies both delta progradation without pronounced avulsion across a deep basin and that the delta circumvented the emergent landmass to reach the Sverdrup Basin. The direct route seems more credible than transport of sediments across an emergent, low-lying landmass. Second, large amounts of sediments prograded over to basins to the NW (Fig. 6) (Klausen *et al.* 2019), and results of the modelling presented here show the potential for the Uralo-Siberian sediment source to supply clastic material across many hundreds of kilometres. In addition, the relatively short distance between the GBSB, Svalbard and the Sverdrup Basin throughout the Triassic (Fig. 1) (Shephard *et al.* 2013) and the late Carnian and late Norian timing of bypass in the GBSB coincide with the timing of the Pat Bay and Hoyle Bay formations (Fig. 3) in the Sverdrup Basin. Third, it is unlikely that a very proximal landmass would supply the fine-grained and well-sorted sandstones observed in the Sverdrup Basin, and no evidence for a northern source or southerly transport directions is observed in time-equivalent strata on Svalbard (e.g. Riis *et al.* 2008; Gilmullina *et al.* 2021b). Finally, the great similarity between the detrital zircon age spectra in the late Carnian and Late Norian of the Sverdrup Basin (Fig. 4k and l) and the GBSB, including Svalbard, shows that the two basins had a common Uralo-Siberian source.

The Urals, Taimyr and Siberia have been suggested as a source for the Triassic sediments in the Sverdrup Basin in previous studies (Omma 2009; Omma *et al.* 2011; Miller *et al.* 2013; Anfinson *et al.* 2016), and the GBSB has even been proposed as an alternative pathway for sediment transport (Anfinson *et al.* 2016). Our data add weight to the idea that the Uralo-Siberian source is the primary source for the Late Triassic sediments in Arctic basins, and that the GBSB is the main sediment route through which the bypass took place (Figs 9–11). Based on the evidence presented above, we suggest that there is no need for an extra sediment source in the middle of the Triassic Arctic, as shown in many reconstructions as a Chukotka–Alaska microcontinent (Sømme *et al.* 2018) or as local highs (Miller *et al.* 2018). In fact, inferring such a terrane sets up an artificial constraint on sediment dispersal patterns and plate reconstructions because models need to account for an 'Arctic Atlantis'. We propose that the Crockerland concept should be abandoned, that a more useful view is that the Arctic basins were connected in the Triassic, and that the Polar Urals together with source areas in West Siberia supplied the majority of the basin-filling sediment, consisting of vast amounts of mudstone-rich sediments with mineralogically immature sandstones and a characteristic detrital zircon age spectrum.

Conclusions

In this study, we present a novel approach, based on sediment budget modelling and support from provenance data, that helps to constrain Arctic sediment transport pathways and improve plate-tectonic and palaeogeographical reconstruction. The source-to-sink approach shows the importance of evaluating sediment bypass and the connectedness of adjacent sedimentary basins, and of using a mass-balance approach. Based on this work, we suggest revisions to the Triassic plate-tectonic reconstruction of the Arctic, although our

interpretation should be tempered by the fact that this is essentially a sedimentological, not geodynamic approach. Future work would ideally include a rigorous geodynamic testing of the ideas presented.

The present study presents a revised, uniform Triassic lithostratigraphy for the Arctic, explaining the sediment supply patterns that created the characteristic detrital zircon spectra found throughout the Triassic within the Arctic sedimentary basins. Results show that the Uralo-Siberian signature was found in detrital zircons across all basins in the Carnian and the Norian, which implies that the Arctic basins were closely connected.

The results imply that the Uralo-Siberian source dominated the Arctic basins in the Late Triassic, and that enigmatic local terranes such as 'Crockerland' or the Pangean 'Rim of Fire' are not needed to explain Arctic sediment supply. Finally, we show how the reconstructed Arctic sediment routing system constrains plate-tectonic models and we offer new plate-tectonic and palaeogeographical reconstructions based on this concept.

Scientific editing by Mary Ford

References

Alonso-Torres, D., Beauchamp, B., Guest, B., Hadlari, T. and Matthews, W. 2018. Late Paleozoic to Triassic arc magmatism north of the Sverdrup Basin in the Canadian Arctic: evidence from detrital zircon U–Pb geochronology. *Lithosphere*, **10**, 426–445, https://doi.org/10.1130/L683.1

Amato, J.M., Toro, J., Akinin, V.V., Hampton, B.A., Salnikov, A.S. and Tuchkova, M.I. 2015. Tectonic evolution of the Mesozoic South Anyui suture zone, eastern Russia: A critical component of paleogeographic reconstructions of the Arctic region. *Geosphere*, **11**, 1530–1564, https://doi.org/10.1130/GES01165.1

Anfinson, O.A., Embry, A.F. and Stockli, D.F. 2016. Geochronologic constraints on the Permian–Triassic northern source region of the Sverdrup Basin, Canadian Arctic Islands. *Tectonophysics*, **691**, 206–219, https://doi.org/10.1016/j.tecto.2016.02.041

Bergan, M. and Knarud, R. 1993. Apparent changes in clastic mineralogy of the Triassic–Jurassic succession, Norwegian Barents Sea: possible implications for palaeodrainage and subsidence. *Norwegian Petroleum Society Special Publications*, **2**, 481–493, https://doi.org/10.1016/B978-0-444-88943-0.50034-4

Brewer, C.J., Hampson, G.J., Whittaker, A.C., Roberts, G.G. and Watkins, S.E. 2020. Comparison of methods to estimate sediment flux in ancient sediment routing systems. *Earth-Science Reviews*, **207**, 103217, https://doi.org/10.1016/j.earscirev.2020.103217

Bue, P.E. and Andresen, A. 2014. Constraining depositional models in the Barents Sea region using detrital zircon U–Pb data from Mesozoic sediments in Svalbard. *Geological Society, London, Special Publications*, **386**, 261–279, https://doi.org/10.1144/SP386.14

Chistyakova, A.V., Veselovskiy, R.V., Semenova, D.V., Kovach, V.P., Adamskaya, E.V. and Fetisova, A.M. 2020. Stratigraphic correlation of Permian–Triassic red beds, Moscow Basin, East European platform: first detrital zircon U–Pb dating results. *Doklady Earth Sciences*, **492**, 306–310, https://doi.org/10.1134/S1028334X20050062

Colpron, M. and Nelson, J.L. 2011. A Palaeozoic NW Passage and the Timanian, Caledonian and Uralian connections of some exotic terranes in the North American Cordillera. *Geological Society, London, Memoirs*, **35**, 463–484, https://doi.org/10.1144/M35.31

Czarniecka, U., Haile, B.G., Braathen, A., Krajewski, K.P., Kristoffersen, M. and Jokubauskas, P. 2020. Petrography, bulk-rock geochemistry, detrital zircon U–Pb geochronology and Hf isotope analysis for constraining provenance: an example from Middle Triassic deposits (Bravaisberget Formation), Sørkappøya, Svalbard. *Norwegian Journal of Geology*, **100**, https://doi.org/10.17850/njg100-3-5

Doré, A.G., Lundin, E.R., Gibbons, A., Sømme, T.O. and Tørudbakken, B.O. 2016. Transform margins of the Arctic: a synthesis and re-evaluation. *Geological Society, London, Special Publications*, **431**, 63–94, https://doi.org/10.1144/SP431.8

Døssing, A., Gaina, C., Jackson, H.R. and Andersen, O.B. 2020. Cretaceous ocean formation in the High Arctic. *Earth and Planetary Science Letters*, **551**, 116552, https://doi.org/10.1016/j.epsl.2020.116552

Egorov, A.U., Bogomolov, Y.A. *et al.* 1987. Stratigraphy of Triassic deposits of Kotelny Island (Novosibirsk Islands). *Boreal Triassic*, M: Nauka, **689**, 66–80 [In Russian].

Eide, C.H., Klausen, T.G., Katkov, D., Suslova, A.A. and Helland-Hansen, W. 2018. Linking an Early Triassic delta to antecedent topography: source-to-sink study of the southwestern Barents Sea margin. *Geological Society of America Bulletin*, **130**, 263–283, https://doi.org/10.1130/B31639.1

Embry, A.F. 1993. Crockerland – the northwest source area for the Sverdrup Basin, Canadian Arctic Islands. *Norwegian Petroleum Society Special Publications*, **2**, 205–216, https://doi.org/10.1016/B978-0-444-88943-0.50018-6

Embry, A. 1997. The Blind Fiord Formation and Blaa Mountain Group (Triassic) of northwestern Axel Heiberg Island, Canadian Arctic Archipelago. *Geological Survey of Canada, Papers*, **97**, 193–198, https://doi.org/10.1130/B31639.1

Embry, A. 2011. Petroleum prospectivity of the Triassic–Jurassic succession of Sverdrup Basin, Canadian Arctic Archipelago. *Geological Society, London, Memoirs*, **35**, 545–558, https://doi.org/10.1144/M35.36

Embry, A. and Beauchamp, B. 2019. Sverdrup basin. *In:* Miall, A.D. (ed.) *The Sedimentary Basins of the United States and Canada*, 2nd edn. Elsevier, Amsterdam, 559–592, https://doi.org/10.1016/B978-0-444-63895-3.00014-0

Ershova, V.B., Prokopiev, A.V., Khudoley, A.K., Sobolev, N.N. and Petrov, E.O. 2015. U/Pb dating of detrital zircons from late Palaeozoic deposits of Bel'kovsky Island (New Siberian Islands): critical testing of Arctic tectonic models. *International Geology Review*, **57**, 199–210, https://doi.org/10.1080/00206814.2014.999358

Fleming, E.J., Flowerdew, M.J. *et al.* 2016. Provenance of Triassic sandstones on the southwest Barents Shelf and the implication for sediment dispersal patterns in northwest Pangaea. *Marine and Petroleum Geology*, **78**, 516–535, https://doi.org/10.1016/j.marpetgeo.2016.10.005

Flowerdew, M.J., Fleming, E.J., Morton, A.C., Frei, D., Chew, D.M. and Daly, J.S. 2019. Assessing mineral fertility and bias in sedimentary provenance studies: examples from the Barents Shelf. *Geological Society, London, Special Publications*, **484**, 255–274, https://doi.org/10.1144/SP484.11

Gaina, C., Werner, S.C., Saltus, R. and Maus, S. 2011. Circum-Arctic mapping project: new magnetic and gravity anomaly maps of the Arctic. *Geological Society, London, Memoirs*, **35**, 39–48, https://doi.org/10.1144/M35.3

Galloway, B.J., Dewing, K., Beauchamp, B. and Matthews, W. 2021. Upper Paleozoic stratigraphy and detrital zircon geochronology along the northwest margin of the Sverdrup Basin, Arctic Canada: insight into the paleogeographic and tectonic evolution of Crockerland. *Canadian Journal of Earth Sciences*, **58**, 164–187, https://doi.org/10.1139/cjes-2019-0226

Gilmullina, A., Klausen, T.G., Doré, A.G., Rossi, V.M., Suslova, A. and Eide, C.H. 2021*a*. Linking sediment supply variations and tectonic evolution in deep time, source-to-sink systems—the Triassic Greater Barents Sea Basin. *Geological Society of America Bulletin*, **134**, 1760–1780, https://doi.org/10.1130/B36090.1

Gilmullina, A., Klausen, T.G., Paterson, N.W., Suslova, A. and Eide, C.H. 2021*b*. Regional correlation and seismic stratigraphy of Triassic strata in the Greater Barents Sea: implications for sediment transport in Arctic basins. *Basin Research*, **33**, 1546–1579, https://doi.org/10.1111/bre.12526

Glørstad-Clark, E., Faleide, J.I., Lundschien, B.A. and Nystuen, J.P. 2010. Triassic seismic sequence stratigraphy and paleogeography of the western Barents Sea area. *Marine and Petroleum Geology*, **27**, 1448–1475, https://doi.org/10.1016/j.marpetgeo.2010.02.008

Gottlieb, E.S., Meisling, K.E., Miller, E.L. and Mull, C.G.G. 2014. Closing the Canada Basin: detrital zircon geochronology relationships between the North Slope of Arctic Alaska and the Franklinian mobile belt of Arctic Canada. *Geosphere*, **10**, 1366–1384, https://doi.org/10.1130/GES01027.1

Hadlari, T., Midwinter, D., Galloway, J.M., Dewing, K. and Durbano, A.M. 2016. Mesozoic rift to post-rift tectonostratigraphy of the Sverdrup Basin,

Canadian Arctic. Marine and Petroleum Geology, **76**, 148–158, https://doi.org/10.1016/j.marpetgeo.2016.05.008

Hadlari, T., Midwinter, D., Poulton, T.P. and Matthews, W.A. 2017. A Pangean rim of fire: reviewing the Triassic of western Laurentia. *Lithosphere*, **9**, 579–582, https://doi.org/10.1130/L643.1

Haile, B.G., Klausen, T.G., Jahren, J., Braathen, A. and Hellevang, H. 2018. Thermal history of a Triassic sedimentary sequence verified by a multi-method approach: Edgeøya, Svalbard, Norway. *Basin Research*, **30**, 1075–1097, https://doi.org/10.1111/bre.12292

Haile, B.G., Line, L.H., Klausen, T.G., Olaussen, S., Eide, C.H., Jahren, J. and Hellevang, H. 2021. Quartz overgrowth textures and fluid inclusion thermometry evidence for basin-scale sedimentary recycling: An example from the Mesozoic Barents Sea Basin. *Basin Research*, **33**, 1697–1710, https://doi.org/10.1111/bre.12531

Houseknecht, D.W. 2019. Evolution of the Arctic Alaska sedimentary basin. Miall, A.D. (ed.) *The Sedimentary Basins of the United States and Canada*, 2nd edn. Elsevier, Amsterdam, 719–745, https://doi.org/10.1016/B978-0-444-63895-3.00018-8

Jackson, S.E., Pearson, N.J., Griffin, W.L. and Belousova, E.A. 2004. The application of laser ablation-inductively coupled plasma-mass spectrometry to in situ U–Pb zircon geochronology. *Chemical Geology*, **211**, 47–69, https://doi.org/10.1016/j.chemgeo.2004.06.017

Jakobsson, M., Macnab, R. *et al.* 2008. An improved bathymetric portrayal of the Arctic Ocean: implications for ocean modeling and geological, geophysical and oceanographic analyses. *Geophysical Research Letters*, **35**, L07602, https://doi.org/10.1029/2008GL033520

Johannessen, E.P. and Embry, A.F. 1989. Sequence correlation: upper Triassic to lower Jurassic succession, Canadian and Norwegian Arctic. *In: Correlation in Hydrocarbon Exploration*. Springer, Dordrecht, 155–170, https://doi.org/10.1007/978-94-009-1149-9_13

Khudoley, A.K., Sobolev, N.N. *et al.* 2019. A reconnaissance provenance study of Triassic–Jurassic clastic rocks of the Russian Barents Sea. *GFF*, **141**, 263–271, https://doi.org/10.1080/11035897.2019.1621372

Klausen, T.G. and Helland-Hansen, W. 2018. Methods for restoring and describing ancient clinoform surfaces. *Journal of Sedimentary Research*, **88**, 241–259, https://doi.org/10.2110/jsr.2018.8

Klausen, T.G. and Mørk, A. 2014. The Upper Triassic paralic deposits of the De Geerdalen Formation on Hopen: outcrop analog to the subsurface Snadd Formation in the Barents Sea. *AAPG Bulletin*, **98**, 1911–1941, https://doi.org/10.1306/02191413064

Klausen, T.G., Ryseth, A.E., Helland-Hansen, W., Gawthorpe, R. and Laursen, I. 2014. Spatial and temporal changes in geometries of fluvial channel bodies from the Triassic Snadd Formation of offshore Norway. *Journal of Sedimentary Research*, **84**, 567–585, https://doi.org/10.2110/jsr.2014.47

Klausen, T.G., Ryseth, A.E., Helland-Hansen, W., Gawthorpe, R. and Laursen, I. 2015. Regional development and sequence stratigraphy of the Middle to Late Triassic Snadd formation, Norwegian Barents Sea. *Marine and Petroleum Geology*, **62**, 102–122, https://doi.org/10.1016/j.marpetgeo.2015.02.004

Klausen, T.G., Müller, R., Slama, J. and Helland-Hansen, W. 2017. Evidence for Late Triassic provenance areas and Early Jurassic sediment supply turnover in the Barents Sea Basin of northern Pangea. *Lithosphere*, **9**, 14–28, https://doi.org/10.1130/L556.1

Klausen, T.G., Nyberg, B. and Helland-Hansen, W. 2019. The largest delta plain in Earth's history. *Geology*, **47**, 470–474, https://doi.org/10.1130/G45507.1

Klausen, T.G., Rismyhr, B., Müller, R. and Olaussen, S. 2022. Changing provenance and stratigraphic signatures across the Triassic–Jurassic boundary in eastern Spitsbergen and the subsurface Barents Sea. *Norwegian Journal of Geology*, https://doi.org/10.17850/njg102-2-1

Krajewski, K. 2008. The Botneheia Formation (Middle Triassic) in Edgeøya and Barentsøya, Svalbard: lithostratigraphy, facies, phosphogenesis, paleoenvironment. *Polish Polar Research*, **29**, 319–364.

Krajewski, K.P. and Weitschat, W. 2015. Depositional history of the youngest strata of the Sassendalen Group (Bravaisberget Formation, Middle Triassic–Carnian) in southern Spitsbergen, Svalbard. *Annales Societatis Geologorum Poloniae*, **85**, 151–175, https://doi.org/10.14241/asgp.2014.005

Kuzmichev, A.B. 2009. Where does the South Anyui suture go in the New Siberian islands and Laptev Sea?: Implications for the Amerasia basin origin. *Tectonophysics*, **463**, 86–108, https://doi.org/10.1016/j.tecto.2008.09.017

Line, L.H., Müller, R., Klausen, T.G., Jahren, J. and Hellevang, H. 2020. Distinct petrographic responses to basin reorganization across the Triassic–Jurassic boundary in the southwestern Barents Sea. *Basin Research*, **32**, 1463–1484, https://doi.org/10.1111/bre.12437

Lord, G., Solvi, K.H., Ask, M., Mork, A., Hounslow, M. and Paterson, N.W. 2014. The Hopen member: a new member of the Triassic de Geerdalen formation. *Norwegian Petroleum Directorate Bulletin*, **11**, 81–96, https://livrepository.liverpool.ac.uk/id/eprint/3108071

McClelland, W.C., Strauss, J.V. *et al.* 2021. Taters versus sliders: evidence for a long-lived history of strike-slip displacement along the Canadian Arctic transform system (CATS). *GSA Today*, **31**, 4–11, https://doi.org/10.1130/GSATG500A.1

Midwinter, D., Hadlari, T., Davis, W.J., Dewing, K. and Arnott, R.W.C. 2016. Dual provenance signatures of the Triassic northern Laurentian margin from detrital-zircon U–Pb and Hf-isotope analysis of Triassic–Jurassic strata in the Sverdrup Basin. *Lithosphere*, **8**, 668–683, https://doi.org/10.1130/L517.1

Miller, E.L., Toro, J. *et al.* 2006. New insights into Arctic paleogeography and tectonics from U–Pb detrital zircon geochronology. *Tectonics*, **25**, https://doi.org/10.1029/2005TC001830

Miller, E.L., Soloviev, A.V., Prokopiev, A.V., Toro, J., Harris, D., Kuzmichev, A.B. and Gehrels, G.E. 2013. Triassic river systems and the paleo-Pacific margin of northwestern Pangea. *Gondwana Research*, **23**, 1631–1645, https://doi.org/10.1016/j.gr.2012.08.015

Miller, E.L., Meisling, K.E. *et al.* 2018. Circum-Arctic Lithosphere Evolution (CALE) Transect C: displacement of the Arctic Alaska–Chukotka microplate towards the Pacific during opening of the Amerasia Basin of the Arctic. *Geological Society, London, Special Publications*, **460**, 57–120, https://doi.org/10.1144/SP460.9

Moore, T.E., Dumitru, T.A. *et al.* 2002. Origin of the Lisburne Hills–Herald Arch structural belt: Stratigraphic, structural, and fission-track evidence from the Cape Lisburne area, northwestern Alaska. *Geological Society of America, Special Papers*, **360**, 77–110, https://doi.org/10.1130/0-8137-2360-4.77

Mørk, A., Embry, A.F. and Weitschat, W. 1989. *Triassic Transgressive–Regressive Cycles in the Sverdrup Basin, Svalbard and the Barents Shelf, Correlation in Hydrocarbon Exploration*. Springer, Berlin, 113–130.

Mozley, P.S. and Hoernle, K. 1990. Geochemistry of carbonate cements in the Sag River and Shublik Formations (Triassic/Jurassic), North Slope, Alaska: implications for the geochemical evolution of formation waters. *Sedimentology*, **37**, 817–836, https://doi.org/10.1111/j.1365-3091.1990.tb01827.x

Müller, R., Klausen, T.G., Faleide, J.I., Olaussen, S., Eide, C.H. and Suslovad, A. 2019. Linking regional unconformities in the Barents Sea to compression-induced forebulge uplift at the Triassic–Jurassic transition. *Tectonophysics*, **765**, 35–51, https://doi.org/10.1016/j.tecto.2019.04.006

Nikishin, A.M., Petrov, E.I. *et al.* 2019. Geological structure and history of the Arctic Ocean based on new geophysical data: implications for paleoenvironment and paleoclimate. Part 2. Mesozoic to Cenozoic geological evolution. *Earth-Science Reviews*, **217**, 103034, https://doi.org/10.1016/j.earscirev.2019.103034

Nyberg, B., Helland-Hansen, W., Gawthorpe, R., Tillmans, F. and Sandbakken, P. 2021. Assessing first-order BQART estimates for ancient source-to-sink mass budget calculations. *Basin Research*, **33**, 2435–2452, https://doi.org/10.1111/bre.12563

Omma, J.E. 2009. Provenance of late Paleozoic and Mesozoic sediment to key Arctic basins: Implications for the opening of the Arctic Ocean. PhD thesis, University of Cambridge, Cambridge, UK, 222, http://eprints.esc.cam.ac.uk/id/eprint/3086

Omma, J., Pease, V. and Scott, R. 2011. U–Pb SIMS zircon geochronology of Triassic and Jurassic sandstones on northwestern Axel Heiberg Island, northern Sverdrup Basin, Arctic Canada. *Geological Society, London, Memoirs*, **35**, 559–566, https://doi.org/10.1144/M35.37

Paton, C., Woodhead, J.D., Hellstrom, J.C., Hergt, J.M., Greig, A. and Maas, R. 2010. Improved laser ablation U–Pb zircon geochronology through robust downhole fractionation correction. *Geochemistry, Geophysics, Geosystems*, **11**, https://doi.org/10.1029/2009GC002618

Petrov, O.V., Morozov, A.F., Chepkasova, T.V., Kiselev, E.A. and Strelnikov, S.I. 2012. Geological map of Russia and adjoining water areas, 1:2 500 000. Poyasnitelnaya zapiska/Ministry of Natural Resources and Environment of the Russian Federation, Federal Agency for Subsoil Management, Russian Geological Research Institute, A.P. Karpinsky (VSEGEI), 58 [In Russian].

Petrov, O.V., Morozov, A.F. *et al.* 2016. Russian scientific school of geological cartography in compiling new generation of the state geological maps of the Russian Federation, its continental shelf and abyssal oceanic margins of Eurasia and Circumpolar Arctic. *Regional Geology and Metallogeny*, **67**, 6–18 [In Russian].

Petrus, J.A. and Kamber, B.S. 2012. VizualAge: a novel approach to laser ablation ICP-MS U–Pb geochronology data reduction. *Geostandards and Geoanalytical Research*, **36**, 247–270, https://doi.org/10.1111/j.1751-908X.2012.00158.x

Piepjohn, K., Lorenz, H. *et al.* 2018. Mesozoic structural evolution of the New Siberian Islands. *Geological Society, London. Special Publications*, **460**, 239–262, https://doi.org/10.1144/SP460.1

Prokopiev, A.V., Ershova, V.B. *et al.* 2018. Tectonics of the New Siberian Islands archipelago: Structural styles and low-temperature thermochronology. *Journal of Geodynamics*, **121**, 155–184, https://doi.org/10.1016/j.jog.2018.09.001

Richardson, J., Hodgson, D., Paton, D., Craven, B., Rawcliffe, A. and Lang, A. 2017. Where is my sink? Reconstruction of landscape development in southwestern Africa since the Late Jurassic. *Gondwana Research*, **45**, 43–64, https://doi.org/10.1016/j.gr.2017.01.004

Riis, F., Lundschien, B.A., Høy, T., Mørk, A. and Mørk, M.B.E. 2008. Evolution of the Triassic shelf in the northern Barents Sea region. *Polar Research*, **27**, 318–338, https://doi.org/10.1111/j.1751-8369.2008.00086.x

Rossi, V.M., Paterson, N.W., Helland-Hansen, W., Klausen, T.G. and Eide, C.H. 2019. Mud-rich delta-scale compound clinoforms in the Triassic shelf of northern Pangea (Havert Formation, southwestern Barents Sea). *Sedimentology*, **66**, 2234–2267, https://doi.org/10.1111/sed.12598

Shneyder, G.V., Efremova, V.I. and Sedov, V.N. 1989. Stratigraphy and conditions for the formation of Mesozoic deposits of the northeastern tip of the Taimyr Peninsula. *Geological structure and minerals of the northeastern part of the Taimyr Peninsula*. Leningrad, 22–34 [In Russian].

Scotese, C. and Moore, T. 2014. *Atlas of Phanerozoic Temperatures (Mollweide Projection), Volumes 1–6, PALEOMAP Project PaleoAtlas for ArcGIS*. PALEOMAP Project, Evanston, IL, https://doi.org/10.13140/2.1.4904.6086

Sharman, G.R., Sharman, J.P. and Sylvester, Z. 2018. detritalPy: a Python-based toolset for visualising and analysing detrital geo-thermochronologic data. *Depositional Record*, **4**, 202–215, https://doi.org/10.1002/dep2.45

Shephard, G., Müller, D. and Seton, M. 2013. The tectonic evolution of the Arctic since Pangea breakup: integrating constraints from surface geology and geophysics with mantle structure. *Earth-Science Reviews*, **124**, 148–183, https://doi.org/10.1016/j.earscirev.2013.05.012

Sláma, J., Košler, J. *et al.* 2008. Plešovice zircon – a new natural reference material for U–Pb and Hf isotopic microanalysis. *Chemical Geology*, **249**, 1–35, https://doi.org/10.1016/j.chemgeo.2007.11.005

Soloviev, A., Zaionchek, A. *et al.* 2015. Evolution of the provenances of Triassic rocks in Franz Josef Land: U/Pb LA-ICP-MS dating of the detrital zircon from Well Severnaya. *Lithology and Mineral Resources*, **50**, 102–116, https://doi.org/10.1134/S0024490215020054

Sømme, T.O., Martinsen, O.J. and Lunt, I. 2013. Linking offshore stratigraphy to onshore paleotopography: the Late Jurassic–Paleocene evolution of the south Norwegian margin. *Geological Society of America Bulletin*, **125**, 1164–1186, https://doi.org/10.1130/B30747.1

Sømme, T., Doré, A., Lundin, E. and Tørudbakken, B. 2018. Triassic–Paleogene paleogeography of the Arctic: implications for sediment routing and basin fill. *AAPG Bulletin*, **102**, 2481–2517, https://doi.org/10.1306/05111817254

Syvitski, J.P. and Milliman, J.D. 2007. Geology, geography, and humans battle for dominance over the delivery of fluvial sediment to the coastal ocean. *Journal of Geology*, **115**, 1–19, https://doi.org/10.1086/509246

Tevelev, A.V. 2013. Types of posttrappe hypabyssal granitoids of the Circum-Siberian belt. *Moscow University Bulletin, Series 4, Geology*, No. 4 [in Russian].

Tuchkova, M., Sokolov, S. and Kravchenko-Berezhnoy, I. 2009. Provenance analysis and tectonic setting of the Triassic clastic deposits in western Chukotka, northeast Russia. *Stephan Mueller Special Publication Series*, **4**, 177–200, https://doi.org/10.5194/smsps-4-177-2009

Tuchkova, M., Prokopiev, A.V., Khudoley, A. and Verzhbitsky, V.E. 2011. Comparative analysis of Triassic sedimentation in Western Chukotka and south-eastern side of Kular-Nera slate belt (Eastern Verkhoyansk region). *Uchenye Zapiski Kazanskogo Universiteta, Seriya Estestvennye Nauki*, **153** [in Russian], https://doi.org/10.5194/smsps-4-177-2009

Tye, R.S., Bhattacharya, J.P., Lorsong, J.A., Sindelar, S.T., Knock, D.G., Puls, D.D. and Levinson, R.A. 1999. Geology and stratigraphy of fluvio-deltaic deposits in the Ivishak Formation: applications for development of Prudhoe Bay Field, Alaska. *AAPG Bulletin*, **83**, 1588–1623.

Whidden, K.J., Dumoulin, J.A. and Rouse, W.A. 2018. A revised Triassic stratigraphic framework for the Arctic Alaska Basin. *AAPG Bulletin*, **102**, 1171–1212, https://doi.org/10.1306/0726171616517250

Wiedenbeck, M., Allé, P. *et al.* 1995. Three natural zircon standards for U–Th–Pb, Lu–Hf, trace element and REE analyses. *Geostandards Newsletter*, **19**, 1–23, https://doi.org/10.1111/j.1751-908X.1995.tb00147.x

Zakharov, V.A., Rogov, M. and Bragin, N. 2010. *The Russian Arctic during the Mesozoic: stratigraphy, biogeography, paleogeography, and paleoclimate: Russia's Contribution to the International Polar Year 2007/08: Lithospheric Structure and Evolution*. M.: Petersburg, Paulsen Ed., 331–383.

Zhang, J., Covault, J., Pyrcz, M., Sharman, G., Carvajal, C. and Milliken, K. 2018. Quantifying sediment supply to continental margins: application to the Paleogene Wilcox Group, Gulf of Mexico. *AAPG Bulletin*, **102**, 1685–1702, https://doi.org/10.1306/01081817308

Zhang, T., Dyment, J. and Gao, J.Y. 2019. Age of the Canada Basin, Arctic Ocean: indications from high-resolution magnetic data. *Geophysical Research Letters*, **46**, 13712–13721, https://doi.org/10.1029/2019GL085736